Aus der

Berufsgenossenschaftlichen Unfallklinik

Klinik für Unfall- und Wiederherstellungschirurgie

Siegfried Weller Institut für Unfallmedizinische Forschung

Establishment of an in vitro model to analyze the effects of the circadian rhythm on bone metabolism

Inaugural-Dissertation
zur Erlangung des Doktorgrades
der Medizin

der Medizinischen Fakultät
der Eberhard Karls Universität
zu Tübingen

vorgelegt von

Gao, Xiang

2025

Dekan: Professor Dr. B. Pichler

1. Berichterstatter: Professor Dr. A. Nüssler
2. Berichterstatter: Privatdozent Dr. Dr. S. Hoefert

Tag der Disputation: 08.12.2025

Table of contents

1. Introduction ····· 1
1.1. The circadian rhythm and related research ····· 1
1.1.1. Definition of the circadian rhythm ····· 1
1.1.2. SCN and synchronization ····· 2
1.1.3. Circadian rhythm genes and feedbook loops ····· 3
1.1.4. Circadian rhythm–related research ····· 5
1.1.5. The limitations of studying the circadian rhythm of osteoblasts and osteoclasts in animal models ····· 5
1.1.6. The limitations of studying the circadian rhythm of osteoblasts and osteoclasts in human blood models ····· 6
1.2. The relationship between the circadian rhythm and disease ····· 6
1.3. The circadian rhythm of bone cells ····· 7
1.4. Differentiation and metabolism of bone cells ····· 7
1.5. *In vitro* co-culture models of bones cells ····· 9
1.5.1. 2D *in vitro* osteoblast-osteoclast co-culture model ····· 9
1.5.2. 3D *in vitro* osteoblast-osteoclast co-culture model ····· 9
1.6. Composition of human serum ····· 11
1.7. Aim of the study ····· 13
2. Materials and methods ····· 15
2.1. Materials ····· 15
2.1.1. Equipment ····· 15
2.1.2. Consumables ····· 16
2.1.3. Chemicals ····· 17
2.1.4. Solutions ····· 18
2.2. Methods ····· 21
2.2.1. Preparation of human serum pool ····· 21
2.2.2. Cell lines ····· 22
2.2.3. *In vitro* osteoblast-osteoclast co-culture model with FCS ····· 22
2.2.4. *In vitro* 2D osteoblast-osteoclast co-culture model with human serum 23
2.2.5. Preparation of PRP scaffolds ····· 23
2.2.6. *In vitro* 3D osteoblast-osteoclast co-culture model with human serum 24

2.2.7. Resazurin conversion assay ····· 25
2.2.8. Sulforhodamine B (SRB) staining ····· 25
2.2.9. Carbonic anhydrase II (CA II) activity ····· 25
2.2.10. Tartrate-resistant acidic phosphatase (TRAP) activity assay ····· 26
2.2.11. Alkaline phosphatase (AP) activity ····· 26
2.2.12. Alizarin Red staining ····· 26
2.2.13. Stiffness of the PRP scaffolds ····· 27
2.2.14. Mineral content of the PRP scaffolds ····· 27
2.2.15. qRT-PCR ····· 28
2.2.16. Statistics ····· 29
3. Results ····· 31
3.1. The stability of housekeeping genes in samples ····· 31
3.2. The circadian gene expression pattern in the *in vitro* co-culture model with FCS 32
3.3.1. The effects of different human serum concentrations on cell growth in the 2D *in vitro* co-culture model ····· 33
3.3.2. The effects of different human serum concentrations on osteoblast and osteoclast function in the 2D *in vitro* co-culture model ····· 34
3.4.1. The effects of 1% human serum collected at different times of the day on cell growth in the 2D *in vitro* co-culture model ····· 35
3.4.2. The expression of cell proliferation and growth genes in the 2D *in vitro* co-culture model ····· 36
3.4.3. The effects of 1% human serum collected at different times of the day on osteoblast and osteoclast function in the 2D *in vitro* co-culture model ····· 37
3.5. Differences in the formation of bone calcium matrix between the 2D and 3D co-culture models ····· 38
3.6. The expression of circadian rhythm genes in the 2D *in vitro* co-culture model 39
4. Discussion ····· 41
4.1. The use of FCS in the *in vitro* co-culture model could not demonstrate the circadian rhythm. ····· 41
4.2. Determination of the optimal human serum concentration to replace FCS 42

4.3. The circadian rhythm in the in vitro co-culture model with human serum collected in the morning, afternoon, and evening ····· 43
4.3.1. Osteoblast and osteoclast growth in the 2D co-culture ····· 43
4.3.2. Osteoblast and osteoclast differentiation and function in the 2D co-culture 43
4.3.3. Osteoblast and osteoclast differentiation and function in the 3D co-culture 45
4.4. Evaluation of the reliability of the *in vitro* co-culture model to represent the circadian rhythm. ····· 46
4.5. Limitations ····· 46
4.6. Outlook ····· 47
4.7. Conclusion ····· 48
5.1. Summary ····· 50
5.2. Zusammenfassung ····· 52
6. Bibliography ····· 54
7. Declaration ····· 62
8. Acknowledgements ····· 63

List of figures

Figure 1 The circadian rhythm in human body and tissues 2
Figure 2 The central circadian rhythm in the SCN synchronizes the peripheral circadian rhythms of organs and tissues 3
Figure 3 Positive and negative loops of circadian gene expression 5
Figure 4 The differentiation of osteoblasts and osteoclasts..... 8
Figure 5 Establishment of the *in vitro* 2D and 3D osteoblast-osteoclast co-cultures 10
Figure 6 Human blood sample collection..... 21
Figure 7 Preparation of PRP scaffolds 24
Figure 8 Analysis of CT images with ImageJ..... 27
Figure 9 Stability of the four housekeeping genes in the samples 31
Figure 10 Circadian gene expression in the co-culture model with FCS 32
Figure 11 The growth of cells is promoted by the presence of human serum in the 2D co-culture model 33
Figure 12 Osteoblast function and osteoclast differentiation and function 35
Figure 13 The impact of human serum collected at three times of the day on bone cell growth 36
Figure 14 The effects of human serum collected in the morning, afternoon, and evening on the expression of genes related to cell proliferation and growth 37
Figure 15 The effects of human serum collected in the morning, afternoon, and evening on osteoclast and osteoblast differentiation and function 38
Figure 16 Analysis of the extracellular calcium matrix in in the 2D and 3D *in vitro* models 39
Figure 17 The expression of circadian rhythm genes in the 2D co-culture model.... 40
Figure 18 The circadian rhythm of osteoblasts and osteoclasts..... 51
Abbildung 19 Der zirkadiane Rhythmus von Osteoblasten und Osteoklasten 53

List of tables

Table 1 List of equipment 15
Table 2 List of consumables 16
Table 3 List of chemicals 17
Table 4 List of solutions 18
Table 5 List of the primers used for qRT-PCR 29

List of abbreviations

2D	Two dimensional
3D	Three dimensional
AP	Alkaline phosphatase
BMP	Bone morphogenic protein
$CaCl_2$	Calcium chloride
CA II	Carbonic anhydrase II
CT	Computed tomography
CTX	C-terminal telopeptide of type I collagen
cDNA	Complementary DNA
DMSO	Dimethyl sulfoxide
DPBS	Dulbecco's Phosphate Buffered Saline
DEPC	Diethylpyrocarbonate
EtOH	Ethanol
EDTA	Ethylenediaminetetraacetic acid
FCS	Fetal calf serum
HCl	Hydrogen chloride
IL-6	Interleukin 6
IGF	Insulin-like Growth Factor
M-CSF	Macrophage colony-stimulating factor
MSCs	Marrow mesenchymal stem cells
MEM α	Minimum Essential Medium Eagle alpha
NaCl	Sodium chloride
NaOH	Sodium hydroxide
OPG	Osteoprotegerin
pNPP	Para-nitropheyl-phosphate
PMA	Phorbole-12-myristate-13-acetate
PBS	Phosphate buffered saline
PINP	Procollagen type I N-terminal propeptide
PRP	Platelet-rich plasma
pHEMA	Poly (2-hydroxyethyl methacrylate)
qRT-PCR	Quantitative reverse transcription polymerase chain reaction
RANKL	Receptor activator of nuclear factor kappa-B ligand
SRB	Sulforhodamine B
SCN	Suprachiasmatic nucleus
TRAP	Tartrate-resistant acid phosphatase
TEMED	Tetramethylethylenediamine
TGF-β	Transforming Growth Factor Beta
VEGF	Vascular Endothelial Growth Factor

1. Introduction

1.1. The circadian rhythm and related research

1.1.1. Definition of the circadian rhythm

The circadian rhythm, also known as the biological clock, is a normal physiological phenomenon that exists in mammals, plants, and even microorganisms. In humans, the circadian rhythm is present in the human body from the moment of birth. This natural oscillation repeats approximately every 24 hours and has a major influence on the regulation of human physiology and behavior every day. It is observed in a multitude of human tissues and organs, including the liver, bones, kidneys, muscles, and adipose tissues, among other tissues and cells.

The circadian rhythm comes from the regular change of light–dark conditions in the surroundings, information that is received by the eyes of mammals (including humans) and converted into chemical signals. After being processed by the central suprachiasmatic nucleus (SCN) (Dibner et al., 2010), the melatonin concentration is altered to reflect the changes in light and darkness in the external environment. As an essential part of the internal biological clock, the circadian rhythm governs numerous critical bodily functions, such as the regulation of heart rate and body temperature, and blood pressure, as well as hormone secretion and the regular activities of tissues, organs, and even cells (Figure 1) (Patke et al., 2020).

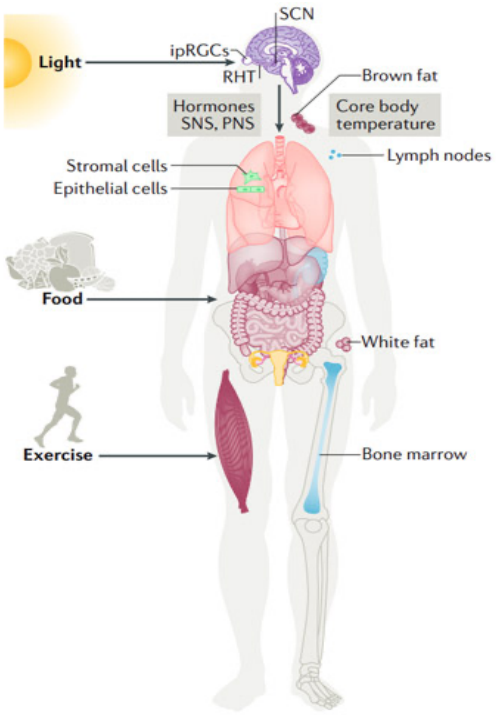

Figure 1 The circadian rhythm in human body and tissues

The circadian rhythm is a fundamental process that exists in all tissues and cells of the human body (muscle, bone, nervous tissue, liver, kidney, lung, stomach, adipose tissue, etc.). It exerts a major influence on the regulation of cellular metabolism and function. At the core of circadian regulation lies the SCN, which functions as responsible for synchronizing the peripheral circadian rhythms. This image has been used with permission from (Patke et al., 2020).

1.1.2. SCN and synchronization

The SCN is a region of the brain situated on both sides of the anterior hypothalamus. It is essential to regulation of the circadian rhythm in the majority of bodily tissues and cells. When the eyes, as visual receptors, sense changes in light intensity in the external environment, they transmit this information to the SCN, which then responds to these changes by altering the central circadian rhythm—via changes in melatonin and other substances— to facilitate the body's adaptation to change in the external light environment (Hastings et al., 2018; Rosenwasser & Turek, 2015). These changes demonstrate regularity and periodicity, typically repeating every 24 hours.

Synchronization is the process by which peripheral tissues and cells maintain synchrony with the circadian rhythm of the SCN. It is currently postulated that the

SCN releases certain circadian rhythm–related substances into the blood, including melatonin, cortisol, parathyroid hormone (PTH), insulin-like growth factor (IGF), growth hormone (GH), and bone conversion factors and markers (which regulate the growth and function of bones cells) (Murck & Steiger, 1998; Rahman et al., 2019; Tsang et al., 2014). Once released into the blood serum, these substances are delivered to various tissues and cells to ensure their circadian rhythm is in phase with that of the SCN and thus consistent with changes in the external environment (Figure 2) (Dibner et al., 2010).

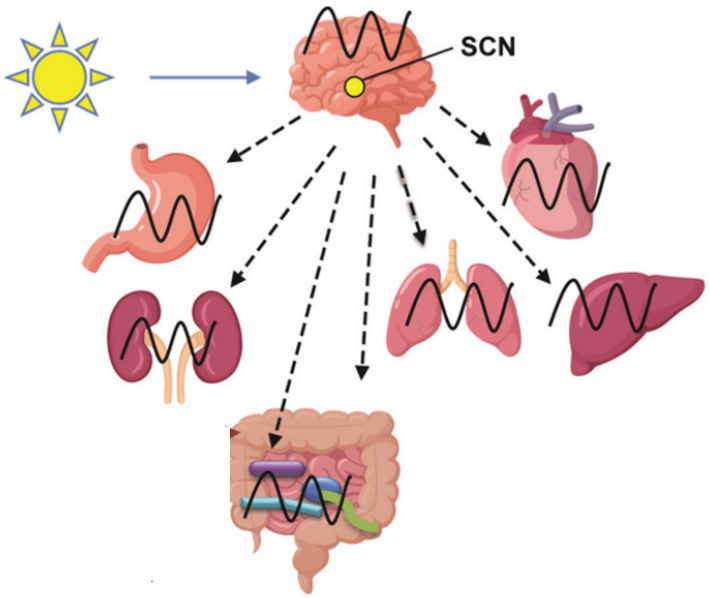

Figure 2 The central circadian rhythm in the SCN synchronizes the peripheral circadian rhythms of organs and tissues

The SCN processes incoming information on changes in surrounding natural illumination and modulates the central circadian rhythm accordingly. Additionally, the SCN synchronizes the peripheral circadian rhythms with the central circadian rhythm. This image has been used with permission from (Liang & FitzGerald, 2017).

1.1.3. Circadian rhythm genes and feedback loops

At birth, mammals and humans express several genes of circadian rhythm, such as CLOCK, BMAL1, NAPS2, CRY1, PER1, and PER2 (Vitaterna et al., 2019), throughout the body. The substances released from the SCN into the blood prompt changes in the level of these genes' expression. It is well recognized accepted that this gene expression pattern aligns with the external light

environment and undergoes modifications in response to alterations in this environment, thereby regulating the periodic changes in tissue and cell functions.

Research has demonstrated that the peak expression of the circadian rhythm genes in mammals typically occurs within a fixed time frame. Specifically, CLOCK, BMAL1, and NPAS2 expression usually peaks between the morning and afternoon; PER1 and PER2 expression is highest between the afternoon and evening; and CRY1 shows an early morning peak (McElderry et al., 2013; Schilperoort et al., 2020; Zvonic et al., 2007).

There are two distinct circadian rhythm gene expression feedback loops, namely positive and negative. The positive loop represents the combined action of CLOCK and BMAL1 with the E-Box element, which activates PER, CRY, and other genes, thereby initiating regular and rhythmic transduction and translation. The negative loop comprises PER and CRY. Once these proteins reach a specific concentration, they inhibit CLOCK and BMAL1 gene expression. This positive and negative loop regulation usually repeats every 24 hours (Figure 3).

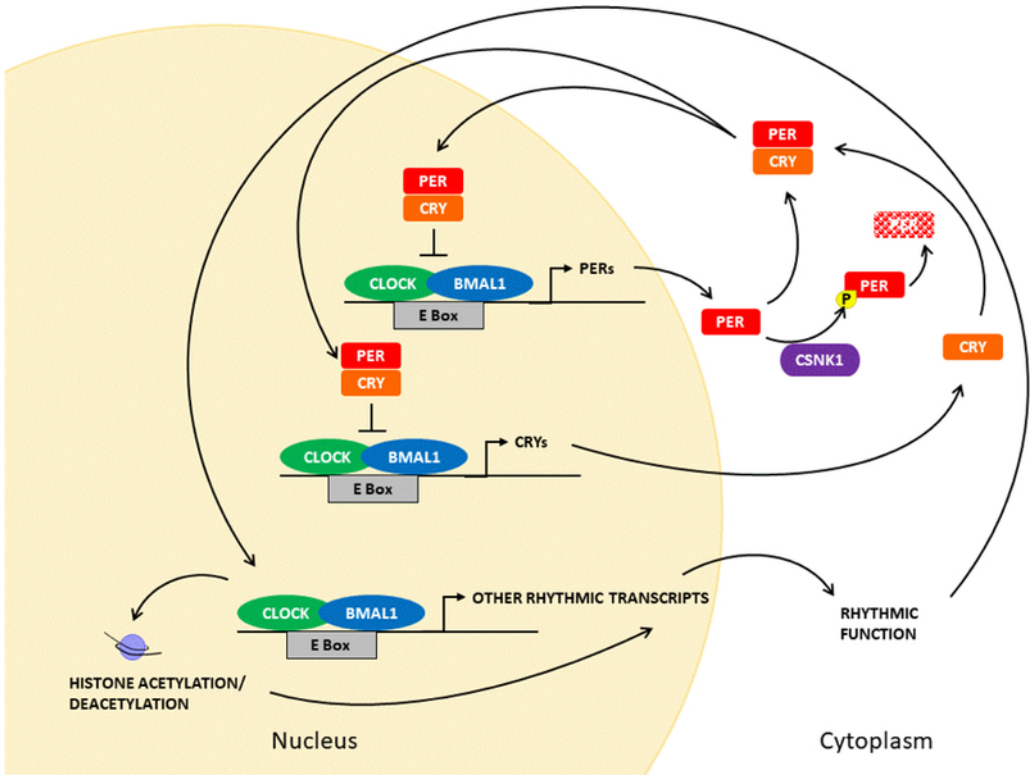

Figure 3 Positive and negative loops of circadian gene expression

The positive loop involves CLOCK and BMAL1. Upon binding to the E-box, CLOCK and BMAL1 activate PER and CRY, thereby initiating transcription and translation. The negative feedback loop includes PER and CRY and their respective protein products. PER and CRY undergo dimerization and subsequently localize to the nucleus, and inhibit CLOCK, BMAL1, and E-box complexes. The positive and negative feedback loops operate alternately within 24 hours and repeat every 24 hours. This image has been used with permission from (Vitaterna et al., 2019).

1.1.4. Circadian rhythm–related research

Since the discovery of the circadian rhythm (Bargiello et al., 1984; Hardin et al., 1990; Zvonic et al., 2007), continuous research has gradually revealed that it is widely present in the human body, participating in and controlling changes in the functions of different organs throughout the body. The research related to the circadian rhythm of human osteoblasts and osteoclasts has mainly utilized animal models to assess changes in the serum levels of bone conversion factors, including insulin-like growth factor (IGF), osteoprotegerin (OPG), receptor activator of nuclear factor kappa-B ligand (RANKL), and procollagen type I N-terminal propeptide (PINP) (Diemar et al., 2023). A main limitation of these studies is the fact that they evaluate the modulation by the circadian rhythm of the growth, differentiation, and function of the osteoblasts and osteoclasts indirectly. New research platforms and methods are needed to directly study and observe the circadian rhythm of human osteoblasts and osteoclasts.

1.1.5. The limitations of studying the circadian rhythm of osteoblasts and osteoclasts in animal models

There are a considerable count of studies that have concentrated on examining the circadian rhythm of human bone cells, but they have used a wide array of models that present various problems. Some of these studies are based on animal models (Schilperoort et al., 2020; Zvonic et al., 2007), and the circadian rhythm of osteoblasts and osteoclasts has been discovered and summarized in animal bone tissue. However, the circadian rhythm of osteoblasts and osteoclasts characterized in animal experiments cannot be regarded as applicable to the circadian rhythm of human osteoblasts and osteoclasts. Indeed, there is no

relevant research showing that there is the same circadian rhythm between different species. Moreover, humans are generally diurnal, whereas commonly used mammalian models have different activity patterns: Mice are generally nocturnal and rabbits are crepuscular. Thus, studying the possible circadian rhythm of human bone cells with animal experiments is not a good choice.

1.1.6. The limitations of studying the circadian rhythm of osteoblasts and osteoclasts in human blood models

Other studies of the circadian rhythm of human bone cells are based on healthy human blood samples. The circadian rhythm of human bone cells is measured or evaluated indirectly: Changes in the concentrations of bone cell conversion factors that promote or inhibit bone cells are measured in blood samples taken during different periods of the day. In the blood, bone morphogenetic protein (BMP), IGF, interleukin 6 (IL-6), and PTH, are the most commonly evaluated factors (Diemar et al., 2023). They are related to both bone-building and bone-breaking activities, and their serum concentrations show a circadian rhythm (Kikyo, 2024). A new experimental model and platform is needed to compensate for the limitations and deficiencies of experimental animal models and human blood in studying the circadian rhythm of human bone cells.

1.2. The relationship between the circadian rhythm and disease

Most human activities take place during the day when there is plenty of light. During the day, the circadian rhythm helps important organs to maintain a stable and regular state to complete various biological activities. In the evening, due to the decrease or even disappearance of light, the SCN adjusts the circadian rhythm, and many organs presents different or even completely opposite biological activities from the daytime. For example, arterial pressure, core temperature, and pulse rate and even blood glucose decrease at night, while the blood levels of hormones such as GH, melatonin, and insulin increase at night. Some people have to work during the dark night and rest during the day. This lifestyle disrupts the normal circadian rhythm, changing the function of various

organs and cells, altering the expression of circadian rhythm genes, and leading to some diseases (Boivin et al., 2022). Indeed, compared with the general population, night shift workers have a significantly higher risk of diabetes (Hannemann et al., 2024; Pan et al., 2011; Sharma et al., 2017), hypertension (Lunde et al., 2020), heart disease (Chellappa et al., 2019), fractures, osteoporosis (Bukowska-Damska et al., 2022; Bukowska-Damska et al., 2020), and tumors (Haus & Smolensky, 2013).

1.3. The circadian rhythm of bone cells

The circadian rhythm of bone cells serves a function in their differentiation and metabolism (Luo et al., 2021). Osteoblasts and osteoclasts show differences in differentiation, metabolism, and function at different times of the day, with peak function in the morning and a decrease in the afternoon and evening. This has been confirmed in animal models (Bouchard et al., 2022; Schilperoort et al., 2020; Staub et al., 1988) and human serum bone turnover studies (Kikyo, 2024; Qin et al., 2023; C. Swanson et al., 2017; C. M. Swanson et al., 2017; van der Spoel et al., 2019).

1.4. Differentiation and metabolism of bone cells

Human bone tissue is primarily composed of a variety of cells, the most significant of which are osteoblasts, the bone-forming cells (Hadjidakis & Androulakis, 2006; Karsenty & Wagner, 2002), and osteoclasts, the bone-resorbing cells (Veis & O'Brien, 2023). These two cell types play an essential part in the remodeling and absorption of bone tissue (Kular et al., 2012). The homeostasis of osteoblasts and osteoclasts serves a function in maintaining normal bone tissue morphology and function (Figure 4) (Siddiqui & Partridge, 2016).

Following differentiation, mesenchymal stem cells (MSCs) give rise to osteoblasts and subsequently transform into osteocytes (Ponzetti & Rucci, 2021). The process is regulated by an amount of cytokines, such as BMPs (Xiao et al., 2007). The synthesis, secretion, and mineralization of the bone matrix are primarily functions of osteoblasts (Harada & Rodan, 2003). Osteoclasts are

crucial bone-resorbing cells with a multinuclear structure. They are generated from hematopoietic stem cells (Bar-Shavit, 2007). Osteoclast function is primarily regulated by RANKL and macrophage colony-stimulating factor (M-CSF) (Boyce, 2013; Ono & Nakashima, 2018). Osteoclasts release lactic acid, citric acid, and other metabolites locally, and the inorganic minerals in the bone tissue are dissolved and absorbed under acidic conditions, thereby exerting bone-resorbing function (Blair, 1998).

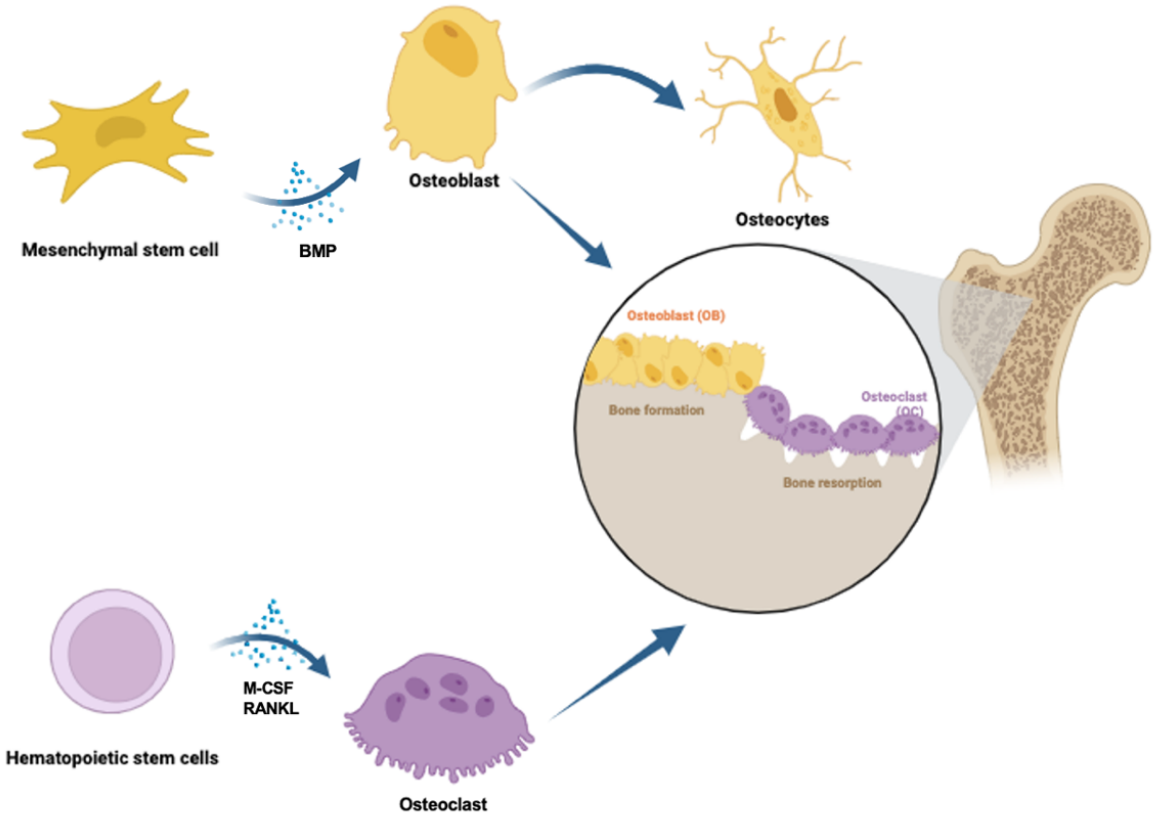

Figure 4 The differentiation of osteoblasts and osteoclasts

MSCs develop into osteoblasts under the influence of osteogenic factors (BMP, etc.) to build bones and ultimately differentiate into osteocytes. Hematopoietic stem cells differentiate into osteoclasts with the assistance of cytokines, including M-CSF and RANKL, which facilitate bone resorption. This image was generated with the assistance of Biorender (https://app.biorender.com/).

1.5. *In vitro* co-culture models of bone cells

1.5.1. 2D *in vitro* osteoblast-osteoclast co-culture model

As noted above, the limitations of animal models and human blood prevent the direct observation of the circadian rhythm of human osteoblasts and osteoclasts. So, *in vitro* cell models have been constructed. For example, researchers have constructed *in vitro* cell models with human fibroblasts and neonatal rat cardiomyocytes to do the research on the circadian rhythm (Francia et al., 2024; Niehoff et al., 2021). In this study, an *in vitro* osteoblast-osteoclast co-culture cell model was used to demonstrate the circadian rhythm (Ehnert et al., 2020; Zhu et al., 2018). Human immortalized mesenchymal stromal cells (SCP-1 cells, which are osteogenic) and monocytic THP-1 cells (osteoclast precursors) were used to construct an *in vitro* co-culture model of the osteoblast-osteoclast (Weng et al., 2021). Previous studies have shown that SCP-1 cells release cytokines such as M-CSF and RANKL during their differentiation into osteoblasts, and these cytokines, along with the addition of phorbole-12-myristate-13-acetate (PMA), can help mononuclear macrophages differentiated from THP-1 cells to further differentiate into osteoclasts (Figure 5). After SCP-1 and THP-1 cells have completed differentiation into osteoblasts and osteoclasts, respectively, the 2D *in vitro* co-culture model of the osteoblast-osteoclast is ready to use.

1.5.2. 3D *in vitro* osteoblast-osteoclast co-culture model

A 2D *in vitro* co-culture models of the osteoblast-osteoclast the interactions between osteoblasts and osteoclasts. However, to simulate a microenvironment that more closely resembles bone cells in the *in vivo* environment, we must also consider cell–matrix interactions. For this reason, researchers have seeded THP-1 and SCP-1 cells on scaffolds made of platelet-rich plasma (PRP) (Figure 5) (Weng et al., 2020). After optimizing the culture medium and plating ratio of the THP-1 and SCP-1 cells, the 3D *in vitro* co-culture model of the osteoblast-osteoclast can maintain the function and viability of the two cell lines.

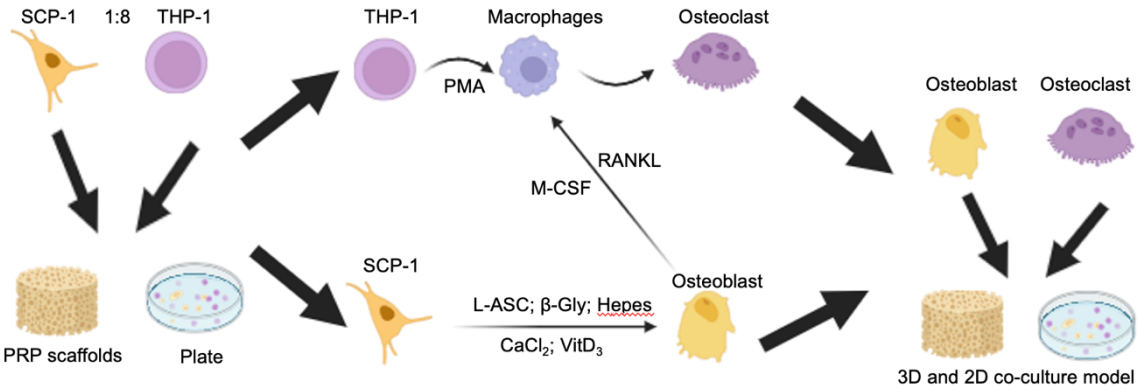

Figure 5 Establishment of the *in vitro* 2D and 3D osteoblast-osteoclast co-cultures

2D and 3D *in vitro* osteoblast-osteoclast co-culture models can be generated with equal cell ratios. In the 2D co-culture model, THP-1 and SCP-1 cells are seeded directly into the wells, and the culture medium is subsequently added. In the 3D co-culture model, the cells are resuspended in 15 µL of culture medium per scaffold and seeded on the scaffolds. After incubation for 4 hours (37°C and 5% CO_2), 500 µL of culture medium is added to each scaffold. In both models, the culture medium is replaced regularly (three times a week) to facilitate the growth and differentiation of the cells. This image was generated with the assistance of Biorender (https://app.biorender.com/).

1.6. Composition of human serum

Human serum, the clear liquid that remains after blood clotting, is a complex mixture of substances. It consists primarily of water, which makes up about 90% of its volume. Serum contains essential proteins, primarily albumin, which supports osmotic balance and substances transports, with globulins including antibodies and transport proteins (Malm et al., 2016). It also contains complement proteins that participate in the immune response. Electrolytes including potassium, sodium, calcium, bicarbonate, magnesium, chloride, and phosphate are essential for maintaining acid-base balance and osmotic pressure. Hormones, which are critical for regulating physiological processes, are also present. Serum carries nutrients such as glucose, amino acids, fatty acids, and vitamins, as well as metabolically generated excretory compounds, such as urea, creatinine, and bilirubin, which must be excreted. It also contains dissolved gases, including oxygen and carbon dioxide; lipids, such as cholesterol and triglycerides; and essential minerals and trace elements, such as iron, zinc, copper, and selenium. The exact concentrations of these components can vary based on individual health, diet, and hydration (Krebs, 1950).

A number of substances have been identified in human serum that are related to osteoblast differentiation. These include PTH, vitamin D (Khundmiri et al., 2016), calcitonin, cortisol, IGF, melatonin, IL-6, and BMP, among others. Additionally, several bone transformation markers are present in serum, including OPG, RANKL, PINP, and CTX (Kulik-Rechberger & Kozlowska, 2024). Research has demonstrated that PTH, GH, IGF, BMP, and bone transformation markers exhibit a pronounced circadian rhythm (Diemar et al., 2023; Luo et al., 2021; Swanson et al., 2018).

Fetal calf serum (FCS) is an animal product that is often used in cell culture experiments. Its main function is to nourish cells and to help them grow and reproduce. The difference between FCS and human serum lies in the nutrients, immune components, and sources they contain. FCS contains more nutrients and higher concentrations of nutrients compared with human serum, and it is

more effective in helping cell growth than human serum. The immune components in human serum are higher in content and more diverse than those in FCS. Finally, FCS comes from animals, while human serum comes from humans. Human serum is more suitable for simulating and constructing the biological environment in the human body, which is especially helpful for experiments that use human cells.

1.7. Aim of the study

The objective of this study was to establish an *in vitro* osteoblast-osteoclast co-culture that can show the circadian rhythm of human bone cells. Below, the two specific aims and the steps performed for each aim are presented.

- Demonstrate the circadian rhythm of human bone cells in an *in vitro* co-culture model of the osteoblast-osteoclast with FCS.
    - ♦ An *in vitro* co-culture model of the osteoblast-osteoclast with FCS and THP-1 and SCP-1 cells was established.
    - ♦ Following incubation for 21 days, RNA was isolated using phenol–chloroform extraction at three distinct time points: morning (7–8 am), afternoon (1–2 pm), and evening (7–8 pm).
    - ♦ Following the isolation of RNA from the co-culture model, the expression patterns of circadian genes was evaluated with quantitative reverse transcription polymerase chain reaction (qRT-PCR).
    - ♦ The results of the expression of biological clock genes were compared with those reported in the literature to assess the reliability of the cell culture model.
- Demonstrate the circadian rhythm of human bone cells in an *in vitro* co-culture model of the osteoblast-osteoclast with human serum collected in the morning, afternoon, and evening.
    - ♦ Human blood was collected from healthy volunteers in the morning (7–8 am), afternoon (1–2 pm), and evening (7–8 pm) on one day. It was centrifuged to obtain serum, which was stored at –80°C.
    - ♦ Different concentrations of the human serum were tested to determine a suitable concentration to replace FCS in the *in vitro* co-culture model of the osteoblast and osteoclast.
    - ♦ Using the optimal concentration, human serum samples collected in morning, afternoon, and evening were employed to construct an *in vitro* osteoblast-osteoclast model and to assess the circadian rhythm.

- RNA was extracted after 21 days of incubation, and qRT-PCR was used to assess the expression of circadian clock genes.
- The circadian gene expression was compared with the literature to evaluate the reliability of the *in vitro* osteoblast-osteoclast co-culture model.

2. Materials and Methods

2.1. Materials

2.1.1. Equipment

Table 1 presents a list of the equipment used for the experiments.

Table 1 List of equipment

Equipment	Manufacturer	Type	Catalog number
Agitator magnetic stirrer	IKA-Werke GmbH	RH B2	06.050357
Agitator, magnetic stirrer	Heidolph Instruments GmbH	MR Hei-Mix L	040700340
Centrifuge	Thermo Fisher Scientific	Megafuge 40R	41307652
Centrifuge	Thermo Fisher Scientific	Fresco 21	30637320
Computed tomography (CT) scanner	Siemens Healthineers	SOMATOM Definition Edge	
Electrophoresis power supply	Bio-Rad Laboratories GmbH	Power Pac 200	285BR05538
Freezer –20°C	BSH	IQ500	GS51NYW41(01)
Freezer –20°C	Liebherr	Med Line	LGex3410-21K001
Freezer –80°C	Thermo Fisher Scientific	905	827860-2521
Fridge +4°C	Liebherr	Comfort	3523-21L
Fridge +4°C	Cool Compact Kühlgerate G	HKMT	040-01 CC00412514
Ice maker	Scotsmen	AF 87	DD 8837 11 X
Incubator	Binder GmbH	9040-0078	11-22649
Incubator	Binder GmbH	9040-0081	11-22190
Laboratory pump (bench)	Carl Roth GmbH+Co.KG	Cyclo 2	1109-065
Microscope	Peqlab Biotechnologie	GmbH EVOS-fl	91-AF-4301
Mixer	Coming Inc	Vortex Mixer	804995
Mixer	Labinco BV	LD- 76	76000
Multichannel pipette	Corning Inc.	5–50 µL	151620022
	Corning Inc.	20–200 µL	551630277
	Corning Inc.	50–300 µL	151640033
Multichannel pipette	Thermo Electron Co.	0.5–10 µL	CH98998 4510
PCR thermal cyclers	Thermo Fisher Scientific	Arktik	10040953
pH meter	Mettler-Toledo GmbH	Five Easy FE 20	1232315296
Pipette controller	Integra GmbH	Pipetboyacu	629619
Pipette controller	Heathrow Scientific LLC	Rota-Filler 3000	HSA05119

Refrigerator	Cool Compact Kuhlgerate G	HKMT 040-01	CC 00412516
	Cool Compact Kuhlgerate G	HKMN 062-01	CC 00412513
Real-time PCR system	Thermo Fisher Scientific	Step One Plus	4376600
Safety workbench	Thermo Fisher Scientific	Maxisave S20201.8	41293949
	Thermo Fisher Scientific	Maxisave S20201.8	41293948
Scale	Kem &Sohn GmbH	ABJ 120-4M	WB 1140084
Shaker, laboratory	LTF Labortechnik GmbH	DRS 12	11DE243, 11DE090
Shaker, laboratory	PeqlabBiotechnologie GmbH	ES-20	010111-1107-0119
Shaker, laboratory	Corning Inc.	LSE Vortex Mixer	1101260
Single-channel pipette	Corning Inc.	0.5–10 µL	158220060
	Corning Inc.	2–20 µL	158230441
	Coming Inc.	10–100 µL	158240031
	Coming Inc.	20–200 µL	158250088
	Corning Inc.	100–1000 µL	058261237
	Eppendorf	0.1–2.5 µL	P35434B
Spectrophotometer	BMG Labtech GmbH	Fluostar Omega	415-1264
Water bath	Lauder Dr.R.Wobser GmbH	AI 25	LCB 0727-11- 0094

2.1.2. Consumables

Table 2 details the consumables that were employed in the experiments.

Table 2 List of consumables

Consumable	Manufacturer	Type	Serial number
Cell culture plastic	Greiner bio-one	96-well plates, flat bottom	655180
	Greiner bio-one	96-well plates, V bottom	651101
Cell culture plastic	Corning Inc	48-well plates, flat bottom	3548
	Corning Inc	6-well-plates, flat bottom	353046
Cell star Tubes	Greiner bio-one	50 mL	227261
	Greiner bio-one	15 mL	188271
Eppendorf tube	SARSTEDT AG	0.5 mL, white	72.699
Eppendorf tube	Carl Roth GmbH + Co.KG	1.5 mL, yellow, white, blue, green, red	4204.1, 4182.1, 4190.1, 4209.1, 4189.1
	Eppendorf	2.0 mL, white	2549

Pipette tips	Sorenson BioScience, Inc.	0.1–10 µL	Colorless
Pipette tips	Sarstedt AG & Co.	2–200 µL	Yellow
Pipette tips	Ratiolab GmbH	100–1000 µL	Blue

2.1.3. Chemicals

Table 3 provides a list of the chemical used in the experiments.

Table 3 List of chemicals

Substance	Article NO.	Company
4-Nitrophenyl acetate (esterase substrate)	N8130-5G	Merck
4-Nitrophenyl phosphate disodium salt hexahydrate (pNPP)	4165.1	Carl Roth
Acetic acid, purity ≥99.0%	20104.298	VWR
Ammonium persulfate	A3678-25G	Merck
Alizarin Red S (C.I.58005)	0348.2	Carl Roth
Ammonium thiocyanate	221988-100g	Merck
Boric acid	6943.1	Carl Roth
Bromophenol blue	A512.1	Carl Roth
Calcium chloride ($CaCl_2$)	CN93.1	Carl Roth
$CaCl_2$	CN93.2	Carl Roth
Cetylpyridinium chloride monohydrate	CN27.1	Carl Roth
Cholecalciferol	95230	Merck
Chloroform	Y015.1	Carl Roth
Dulbecco's phosphate-buffered saline (DPBS)	D8537	Merck
DMEM high glucose	D5796	Merck
Dimethyl sulfoxide (DMSO)	4720.2	Carl Roth
Disodium hydrogen phosphate	T876.1	Carl Roth
Disodium hydrogen phosphate	T876.1	Carl Roth
Diethylpyrocarbonate (DEPC)	K028.3	Carl Roth
Disodium tartrate dihydrate	0254.1	Carl Roth
DPBS without Mg^{2+}	L182-50	Merck
ddH_2O	3175.1	Carl Roth
Ethylenediaminetetraacetic acid (EDTA)	8043.2	Carl Roth
Ethanol (EtOH)	ETO-10000-99-1	SAV
EtOH (100%)	A1613	Applichem
FCS	10270	Thermo Fisher
First Strand cDNA synthesis Kit	K1612	Thermo Fisher
Glycine	3908.2	Carl Roth
Guanidine thiocyanate	0017.1	Carl Roth
Glycerol	G6376-100G	Merck
Glutaraldehyde	3778.1	Carl Roth
Hydrochloric acid (HCl)	N076.1	Carl Roth
Isopropanol	33539	Honeywell

L-Ascorbic acid-2-phosphate sesqui-magnesium salt	A8960-5G	Merck
MEM alpha	AL081A	HiMedia
Magnesium chloride ($MgCl_2$)	M2670	Merck
$MgCl_2$	KK36.2	Carl Roth
N-2-hydroxyethylpiperazine-*N*-2-ethane sulfonic acid (HEPES)	HN78.2	Carl Roth
PMA	AB120297	Abcam
pHEMA	128635-500G	Sigma
RPMI 1640	R8758	Merck
Resazurin sodium salt	199303-1G	Merck
Roti Aqua Phenol	A980.3	Carl Roth
Sodium chloride (NaCl)	S7653	Merck
NaCl	27810.295	VWR
Sodium acetate	X891.2	Carl Roth
Sodium hydroxide (NaOH)	T135.1	Carl Roth
Sodium hydrogen carbonate	6885.2	Carl Roth
Sulforhodamine B (SRB) sodium salt	S1402-1G	Merck
Trypan Blue	CN76.1	Carl Roth
Tris(hydroxymethyl)aminomethane (Tris)	AE15.1	Carl Roth
Trypsin / EDTA	T3924	Merck
Tris base	T1503	Merck
Tetramethylethylenediamine (TEMED)	2367.3	Carl Roth
β-Glycerophosphate disodium salt hydrate	G9422-10	Merck

2.1.4. Solutions

Table 4 provides the recipe and brief instructions for making the solutions that were employed in the experiments.

Table 4 List of solutions

Buffer/mediums/solutions	Composition and handling
10X TBE	108 g (0.89 M) Tris 55 g (0.89 M) boric acid 99.8% pa 40 mL EDTA (0.5 M) pH 8 Adjust the volume to 1 L with ddH_2O
Acetic acid solution (1%)	49.5 mL ddH_2O 1% (500 µL) acetic acid, purity ≥99.0%
ALP activity assay buffer	3.75 g (50 mM) glycine 12.11 g (100 mM) Tris base 95.2 mg (1 mM) $MgCl_2$ 900 mL ddH_2O Adjust pH to 10.5 with NaOH Adjust volume to 1 L with ddH_2O
ALP assay solution	1.3 mg (3.5 mM) pNPP 1 mL ALP activity assay buffer (pH 10.5)
Alizarin Red staining solution (0.5%)	200 mg Alizarin Red S

	40 mL ddH_2O Adjust pH to 4.0
CA II activity assay buffer	75.7 mg (12.5 mM) Tris base 219.2 mg (75 mM) NaCl 40 mL ddH_2O Adjust pH to 7.5 with HCl Adjust volume to 50 mL with ddH_2O
CA II substrate solution	54.3 mg (200 mM) 4-nitrophenyl acetate (esterase substrate) 1.5 mL EtOH (100%)
CA II Assay Solution	10 µL (2 mM) CA II substrate solution (ultrasonic treatment for 30 minutes to dissolve crystals) 1 mL CA II activity assay buffer
Calcium stock solution	139 mg (25 mM) $CaCl_2$ 4 g (1.37 M) NaCl 71.4 mg (15 mM) $MgCl_2$ 45 mL 50 mM Tris buffer Adjust pH to 7.4 Adjust total volume to 50 mL with 50 mM Tris buffer
Calcium phosphate solution	5.98 mg (2.25 mM) disodium hydrogen phosphate 22.2 mg (4 mM) $CaCl_2$ 407.5 mg (140 mM) NaCl Adjust pH to 7.4, adjust total volume to 50 mL with 50 mM Tris buffer
Cetylpyridinium chloride solution (10%)	10 g cetylpyridinium chloride monohydrate 100 mL tap water (not ddH_2O)
Cholecalciferol stock solution	2 mg (200 µg/mL) cholecalciferol 10 mL DMSO
Co-culture medium	250 mL RPMI 1640 medium with L-glutamine 250 mL MEM alpha modification with glutamine and without nucleosides 0.36 mL FCS; 1.8 mL human serum, FCS, or human serum pool 29 mg (200 µM) L-Ascorbic acid-2-phosphate sesqui-magnesium salt 0.54 g (5 mM) β-Glycerophosphate disodium salt hydrate 2.98 g (25 mM) HEPES 83 mg (1.5 mM) $CaCl_2$ 50 µL (20 ng/mL) cholecalciferol stock solution
DEPC H_2O (0.1%)	1 mL DEPC 1 L ddH_2O
EtOH (70%)	35 mL 99% EtOH 15 mL DEPC H_2O
Human serum pool	10 mL pool of 10 donors (1 mL each) – morning group (7–8 am) 10 mL pool of 10 donors (1 mL each) – afternoon group (1–2 pm) 10 mL pool of 10 donors (1 mL each) – evening group (7–8 pm)

HCl	4 M HCl
NaOH	2 M NaOH
NaOH solution (50 mM)	1.25 mL (2 M) NaOH 48.75 mL ddH_2O
PMA Stock Solution (200 µM)	1 mg (200 µM) PMA 8.1 mL DMSO
Phosphate stock solution	78.8 mg (11.1 mM) disodium hydrogen phosphate 176.4 mg (42 mM) sodium hydrogen carbonate 45 mL 50 mM Tris buffer Adjust pH to 7.4 Adjust total volume to 50 mL with 50 mM Tris buffer
PCR loading buffer (5×)	25 mg Bromophenol blue 5 mL (5×) TBE 5 mL (10%) glycerol (20%)
Resazurin stock solution	0.025% (0.125 g) resazurin sodium salt 500 mL DPBS
Resazurin working solution	100 µL resazurin stock solution 1 mL DMEM high glucose (4.5 g/L) with L-glutamine
SCP-1 cell culture medium	500 mL MEM alpha modification with glutamine and without nucleosides 5% (25 mL) FCS – heat inactivated
SRB staining solution	0.4% (0.2 g) SRB sodium salt 50 mL 1% acetic acid solution
Sodium acetate solution (3M)	12.3 g sodium acetate 50 mL ddH_2O Adjust pH to 5
Lab-made TriFast (100 mL)	9.45 g (0.8 M) guanidine thiocyanate 3.04 g (0.4 M) ammonium thiocyanate 3.3 mL (0.1 M) sodium acetate solution (3M) 5 mL (5%) glycerol
THP-1 cell culture medium	500 mL RPMI 1640 medium with L-glutamine 5% (25 mL) FCS – heat inactivated
THP-1 cell plating medium	15 mL THP-1 cell culture medium 15 µL (200 nM) 200 µM PMA stock solution
Trypan blue solution	62.5 mg trypan blue 50 mL DPBS
TRAP activity assay buffer	8.2 g (100 mM) sodium acetate 11.5 g (50 mM) disodium tartrate dihydrate 900 mL ddH_2O Adjust pH to 5.5 with HCl Adjust volume to 1 mL with ddH_2O
TRAP assay solution	1.9 mg (5 mM) pNPP 1 mL TRAP activity assay buffer (pH 5.5)
Tris buffer	3.02 g (50 mM) Tris base 450 mL ddH_2O Adjust pH to 7.4 with HCl Adjust total volume to 500 mL with ddH_2O
Tris/NaOH mix (DNA measurement)	100 µL 50 mM NaOH 100 µL ddH_2O 10 µL (1 M) Tris pH 8

Tris solution pH 8	6.06 g (1 M) Tris 40 mL ddH_2O Adjust pH to 8.0 with HCl Adjust volume to 50 mL with ddH_2O
Unbuffered Tris solution (10 mM)	10 mM (1.2 g) Tris (hydroxymethyl) aminomethane 1 L ddH_2O

2.2. Methods

2.2.1. Preparation of human serum pool

Figure 6 shows a schematic of the sample collection procedure. A total of 10 healthy young volunteers participated in the study, with blood samples collected from each participant in the morning (7–8 am), afternoon (1–2 pm), and evening (7–8 pm). Each volunteer provided two blood samples on each of the designated occasions. At each time point, approximately 15 mL of blood was collected from each participant. The blood was incubated at 20°C for 30 minutes after that the blood samples was centrifuged at 2000 g (10 minutes, at 20°C), yielding approximately 3 mL of serum. The serum was stored at –80°C until use.

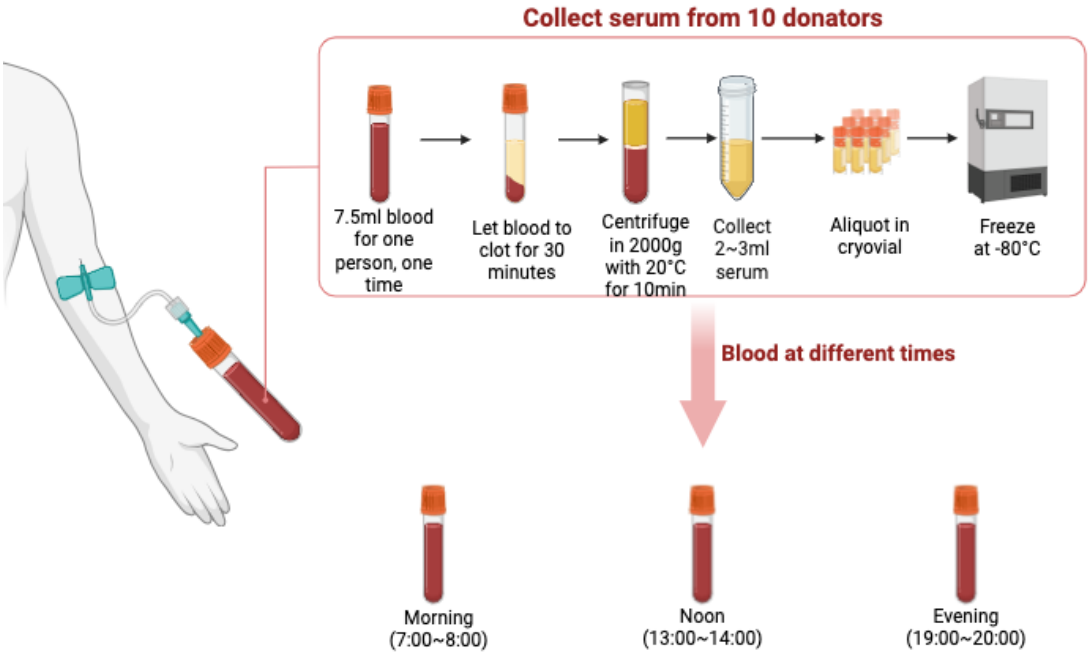

Figure 6 Human blood sample collection

Collected blood samples from the same cohort of healthy volunteers (N = 10) at three time points on the same day: 7–8 am, 1–2 pm, and 7–8 pm. The same quantity of blood was drawn from the same subjects and subjected to centrifugation to obtain serum samples of identical composition. The image was generated with the assistance of Biorender (https://app.biorender.com/).

2.2.2. Cell lines

Immortalized SCP-1 cells, osteoprogenitor cells (Bocker et al., 2008), and human THP-1 cells, osteoclast progenitor cells (Haussling et al., 2021), were used. SCP-1 cells cultures were established using α-Minimum Essential Medium (MEM α) containing 5% (v/v) FCS. THP-1 cells were grown in RPMI 1640 medium enriched with 5% FCS (growth medium). Both cell lines were sustained in an incubator set to 37°C (5% CO_2, humidified atmosphere); the medium was changed twice a week.

2.2.3. *In vitro* osteoblast-osteoclast co-culture model with FCS

The standard 2D and 3D co-culture model of the osteoblast-osteoclast includes FCS, THP-1 cells, SCP-1 cells, PMA, and a 50:50 differentiation medium. THP-1 and SCP-1 cells were seeded in 96-well plates (2D cell model) or on scaffolds (3D cell model) at varying densities but with an identical ratio (8:1). The model was incubated for 14 days to allow the THP-1 cells to transform into macrophages and the SCP-1 cells to transform into osteoblasts. PMA was added to help differentiate the THP-1 cells into macrophages. Moreover, RANKL and M-CSF released from the cells facilitated the differentiation of macrophages into osteoclasts. Although FCS contains numerous bone conversion factors and markers, its primary function is to provide nutritional support during this period, ensuring the normal growth, reproduction, and differentiation of cells.

When the culture medium is refreshed three times a week, the 2D osteoblast-osteoclast *in vitro* co-culture model typically maintains a stable state for 21 days. In contrast, the 3D osteoblast-osteoclast *in vitro* co-culture cell model can maintain a stable state for more than 21 days because the scaffolds generate a spatially organized microenvironment that more closely resembles the *in vivo* bone environment. The 2D and 3D osteoblast-osteoclast *in vitro* co-culture models with FCS exhibit straightforward and stable characteristics, which enable the simulation of osteoblast and osteoclast behavior within a biological context.

2.2.4. *In vitro* 2D osteoblast-osteoclast co-culture model with human serum

SCP-1 and THP-1 cells (up to passage 20) were co-cultured in 96-well plates (Weng et al., 2021). THP-1 cells (2.4×10^4 cells/ 100 µL per well) were plated in RPMI 1640 medium containing 200 nM PMA. The next day, the growth medium was removed, and SCP-1 cells (3×10^3 cells/100 µL per well) were planted in the same well in osteogenic differentiation medium containing 1% human serum (the composition is shown in Table 4). The model was incubated at 37°C (5% CO_2, humidified atmosphere) and the medium were changed three times a week.

2.2.5. Preparation of PRP scaffolds

Figure 7 provides a schematic for the preparation of PRP scaffolds. Briefly, EDTA-treated blood samples collected from the healthy volunteers were centrifuged at 1000 *g* for 10 minutes to isolate PRP. A precursor solution was prepared with 16.0% pHEMA (128635-500G, Sigma), 0.3% *bis*-acrylamide (3039.1, Carl Roth), and 0.25 g/L PRP. After cooling on ice for 30 minutes, the solution was adjusted to a final concentration of 0.3 M by adding disodium hydrogen phosphate buffer (T876.1, Carl Roth).

Crosslinking agents— 0.1% glutaraldehyde (3778.1, Carl Roth), 0.2% ammonium persulfate (A3678-25G, Sigma), and 0.2% tetramethylethylenediamine (TEMED) (2367.3, Carl Roth), were added before pouring the mixture into polystyrene molds (2 mL per mold). The solution was frozen at −18 °C for ≥12 hours, then cooled to −80 °C for 1 hour to create a porous structure via ice crystal templating. The scaffolds measured ~3 mm in height and 6 mm in diameter.

For mineralization, the scaffolds were incubated in a 1 M $CaCl_2$ (CN93.2, Carl Roth) solution for 24 hours to promote the crystallization of calcium phosphate, specifically hydroxyapatite. After removing the $CaCl_2$ solution, the scaffolds were washed with phosphate-buffered saline (PBS; L182-50, Merck) for 15 minutes. In this process, the formation of ice crystals functioned as placeholders, thereby facilitating the creation of the desired pores.

To sterilize the scaffolds and to eliminate potential toxins, after removing PBS, the scaffolds were immersed in a 70% EtOH solution for 12 hours and then were washed with PBS in four stages (30, 60, 90, and 120 minutes). The scaffolds were cultured in THP-1 medium at 37°C and 5% CO_2 for 48 hours as a sterility control (Haussling et al., 2019).

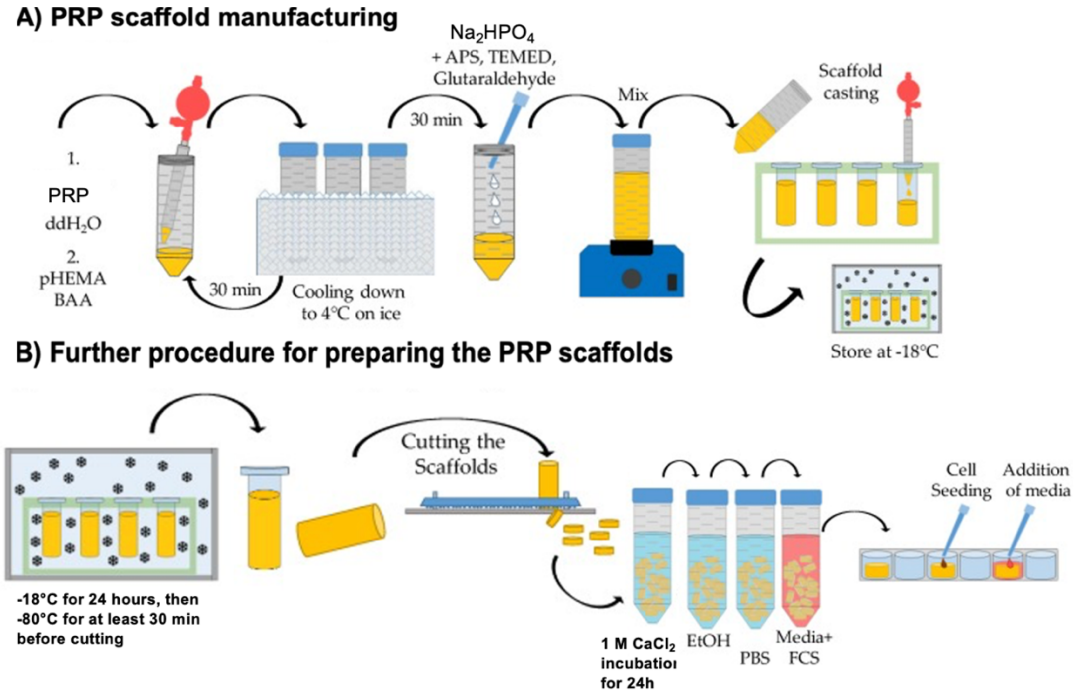

Figure 7 Preparation of PRP scaffolds

(A) The methodology for the fixation and shaping of PRP scaffolds. (B) The process of cutting the scaffolds to size, sterilizing them, and seeding cells on the scaffolds. This image has been used with permission from (Ruoss et al., 2020).

2.2.6. *In vitro* 3D osteoblast-osteoclast co-culture model with human serum

A THP-1 cell suspension (8×10^4 cells/15 µL per scaffold) was seeded on top of the PRP scaffolds (Guo et al., 2022). After incubation at 37°C for 4 hours, 500 µL of growth medium containing 200 nM PMA was gently added. The next day, the growth medium was taken away before cell seeding the SCP-1 cells (1×10^4 cells/15 µL per scaffold) onto the same scaffold. After 4 hours, 500 µL of osteogenic differentiation medium containing 1% human serum was added. The scaffolds and cells were maintained in an incubator at 37°C (5% CO_2, humidified atmosphere); the medium was changed three times a week.

2.2.7. Resazurin conversion assay

Resazurin conversion is a commonly used method to indirectly assess cell proliferation, viability, and toxicity in various types of cells, bacteria, and fungi. The assay relies on the capacity of viable cells to reduce the redox-sensitive dye resazurin into resorufin, a fluorescent and colorimetric end product. To detect mitochondrial activity, cells were washed once with PBS and then 100 µL of 0.0025% (w/v) resazurin working solution was added. The fluorescence was measured at 544 nm/590-10 nm using an Omega plate reader at four time points: 30, 60, 90, and 120 minutes (McMillian et al., 2002; Weng et al., 2020).

2.2.8. Sulforhodamine B (SRB) staining

SRB, a dye that binds to surface proteins under acidic conditions, was utilized to detect total protein in bone cell co-culture in 96-well plates, cells were fixed with 100% EtOH (50 µL/well) at –20°C for at least 1 hour. After removing excess EtOH then washing the cells with tap water for one time, the cells were fixed with SRB solution for 30 minutes on a shaker protected from the light. Then, the cells were washed 3–4 times with 1% acetic acid to remove excess SRB solution. SRB bound to the cells was solubilized by adding 10 mM unbuffered Tris solution. The absorbance was quantified at 544 nm/590-10 nm using an Omega plate reader (Skehan et al., 1990).

2.2.9. Carbonic anhydrase II (CA II) activity

CA II catalyzed the interconversion between CO_2 and H_2O and HCO_3^- and H^+. CA II is expressed during the early stage of the differentiation of osteoclast, and its activity could reflect the degree of osteoclast differentiation and the resorptive activity of osteoclasts, so CA II was used to detect the initial phases of osteoclast differentiation in osteoblast-osteoclast co-cultures, then washed cells once with PBS and then fresh CA II reaction buffer (100 µL/well) prepared on the day of the assay was added. The absorbance at 405 nm was measured immediately for a total of 15 minutes using an Omega plate reader (Bernhardt et al., 2017).

2.2.10. Tartrate-resistant acidic phosphatase (TRAP) activity assay

TRAP is a member of the ubiquitously expressed acid phosphatase family. Osteoclasts are the only human cells that have the ability to resorb bone. During this process, they produce TRAP; therefore, this enzyme is a specific marker for osteoclast activity. The supernatant was collected (30 µL/well) and combined with TRAP substrate buffer solution (90 µL/well) into a fresh 96-well plate then incubated the supernatant at 37°C for 6 hours. To stop the reaction, 1 M NaOH was added to the well (90 µL/well). The absorbance at 405 nm was measured using an Omega plate reader (Burstone, 1959; Minkin, 1982).

2.2.11. Alkaline phosphatase (AP) activity

AP is an enzyme that is produced in the liver, bone, and placenta. It is usually found in high levels in growing bones and bile. Consequently, the measurement of AP activity can be utilized to characterize osteoblast function. To detect osteoblast function, washed cells with PBS for one time, and then AP substrate solution (100 µL/well) was added. After incubation at 37°C for 2 hours, the absorbance at 405 nm using an Omega plate reader (Ehnert et al., 2010; Wildemann et al., 2004).

2.2.12. Alizarin Red staining

Alizarin Red staining was employed to detect the calcium matrix in the osteoblast-osteoclast co-cultures. This compound is routinely applied in biological experiments owing to its ability to stain free calcium and certain calcium compounds a red or light purple color. A key benefit of Alizarin Red is its quantitative accessibility, which can be readily measured through photometric analysis following the dissolution of the dye in a cetylpyridinium chloride solution. To detect extracellular mineralized matrix in bone cells co-culture, cells were fixed with 100% EtOH (50 µL/well) for 60 min at –20°C. After removing excess EtOH and washing three times with tap water, 0.5% Alizarin Red staining solution (50 µL/well) was added, and the plate was incubated for 30 min on a shaker under

the light. Excess solution was taken away, and each well was washed with tap water for three times. After air-drying, cetylpyridinium chloride solution was added, and the plate was incubated for 60 minutes on a shaker. The absorbance at 560 nm was measured with an Omega plate reader.

2.2.13. Stiffness of the PRP scaffolds

An analysis was conducted to measure the stiffness of the PRP scaffolds based on Young's modulus (Weng et al., 2020). A ZwickiLine Z 2.5TN machine vertically compressed the surface scaffolds at a rate of 0.08 mm per second. The applied force was continuously recorded by a force sensor. The stiffness of the PRP scaffolds was calculated as follows:

$$\text{Young's modulus [MPa]} = \frac{applied\ force\ [N] * initial\ scaffold\ height\ [mm]}{area\ of\ the\ scaffold\ [\text{mm}^2] * change\ in\ height\ [mm]}$$

2.2.14. Mineral content of the PRP scaffolds

The mineral content of the PRP scaffolds was determined by quantitative computed tomography (CT) using a high-end clinical 128-slice CT scanner. The resulting stacked images were cropped using the ImageJ software to show the area where the scaffolds were located. The optical density (grayscale) of each scaffold was calculated and standardized using the reference block (phantom EFP-06-96) (Weng et al., 2020). Figure 8 provides an example of this analysis.

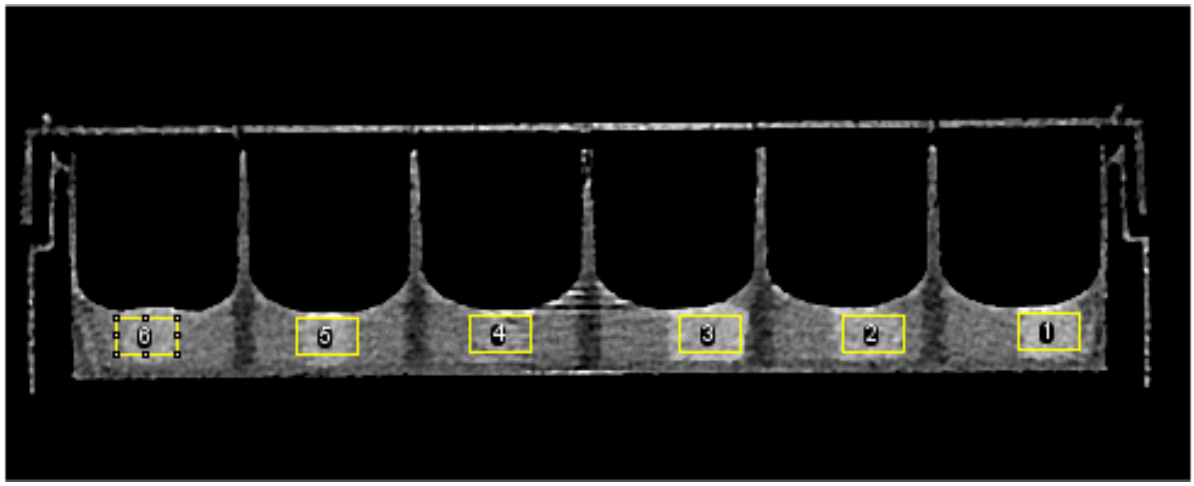

Figure 8 Analysis of CT images with ImageJ

In the same bracket area, gray value analysis was performed using ImageJ software within the specified region. The average value was used for for comparison and evaluation of the difference in mineral density within the bracket.

2.2.15. qRT-PCR

Total RNA was isolated from the osteoblast-osteoclast co-cultures by using a published phenol chloroform extraction protocol (Rodriguez-Ezpeleta et al., 2009). Spectrophotometric methods were employed to determine RNA concentration, and complementary DNA (cDNA) was synthesized using the First Strand cDNA Synthesis Kit, which contains Primer oligo dT, random hexamer primer, 5× reaction buffer, Ribolock RNase Inhibitor, 10 mM dNTP Mix, and M-MULV Reverse Transcriptase. First, 4.5 µL of diluted RNA, 0.5 µL of Primer oligo dT (0.5 µg/µL), and 0.5 µL of the random hexamer primer (0.2 µg/µL) were incubated in a thermal cycler at 65°C for 5 minutes. After cooling the mixture to 4°C, the following were added: 2 µL of 5× reaction buffer, 0.5 µL of Ribolock RNase Inhibitor (20 U/µL), 1 µL of 10 mM dNTP Mix and 1 µL of M-MULV Reverse Transcriptase (20 U/µL). The reaction was incubated at 25°C for 5 minutes; 37°C for 60 minutes; 70°C for 5 minutes and cool down to 4°C in the end.

qRT-PCR was undertaken to investigate the expression of genes associated with the circadian rhythm (BMAL1, CLOCK, NPAS2, CRY1, PER1, PER2) and cell proliferation and growth (MKI67, TOP2A, TPX2) in the osteoblast-osteoclast co-cultures. qRT-PCR with SYBR Green was conducted using 10 ng of the cDNA template with the Biozym Ready Mix. Several housekeeping genes—RPL13a, EF1a, GAPDH, and B2M—were evaluated to determine which is most suitable for qRT-PCR analysis. This investigation involved the osteoclast-osteoblast co-cultures exposed to human serum as well as FCS to assess working temperature, cycle number, and stability. The data were analyzed by using the delta Ct (ΔCt) method, BestKeeper, GeNorm, and NormFinder (Aspera-Werz et al., 2022), in conjunction with the RefFinder tool (Xie et al., 2023). As indicated by this analysis, B2M was selected the most suitable housekeeping gene. Table 5 lists the primers and conditions used for each gene.

Table 5 List of the primers used for qRT-PCR

Gene	Accession Number	Forward primer (5'→3')	Reverse primer (3'→5')	Product length (base pairs)	Efficiency	Annealing temp (°C)	Number of cycles
CLOCK	NM_001267843.2	ACGCACACATAGGCCATCTT	ATTATGGGTGGTGCCCTGTG	177	1.02	66	40
BMAL1	NM_001351814.2	TCCTTTGTTGTAGGTGGCCC	GCGATGACCCTCTTATCCTGT	139	1.12	66	40
NPAS2	NM_002518.4	ACACTCGGTGGTCAGTTACG	CCGATGGCGAATGACTGGTA	188	1.10	66	40
CRY1	NM_001413460.1	CCCAGGTTGTAGCAGCAGTG	AGGACGTTTCCCACCACTTG	111	1.55	60	40
PER1	NM_002616.3	GGGGACCAAGAAAGATCCGC	GCTACACTGACTGGTGACGG	145	0.97	64	40
PER2	XM_054344396.1	CATCGACGTGGCAGAATGTG	ACGTCTGCTCTTCGATCCTG	161	0.80	60	40
B2M	NM_004048.2	AGATGAGTATGCCTGCCGTG	GCGGCATCTTCAAACCTCCA	105	1.01	60	40
RPL13a	NM_012423.3	AAGTACCAGGCAGTGACAG	CCTGTTTCCGTAGCCTCATG	100	1.09	56	40
GAPDH	NM_008084.3	GGACTGGATAAGCAGGGCG	GCCAAATCCGTTCACACCG	196	1.26	56	40
EF1a	NM_001402.5	CCCCGACACAGTAGCATTTG	TGACTTTCCATCCCTTGAACC	98	0.89	56	40
MKI67	NM_002417.5	CGTCCCAGTGGAAGAGTTGT	CGACCCCGCTCCTTTTGATA	143	1.02	63	40
TPX2	NM_012112.5	GGAAGCACCAGCTGGAAGA	GAACTAGAGAACCAGAAAGGCCC	147	1.10	63	40
TOP2A	NM_001067.4	GTTCTTGAGCCCCTTCACGA	ACCCACATTTGCTGGGTCA	216	1.23	63	40

2.2.16. Statistics

Three independent experiments were conducted, with each item repeated at least three times. Differences between multiple groups were evaluated using non-parametric version of a two-way ANOVA or the Kruskal–Wallis test. A p-value < 0.05 was considered to indicate statistical significance. The data were processed

using z-score [1] and ddCT, then analyzed using GraphPad Prism version 9 (GraphPad Software, San Diego, CA, USA). The data are presented as diagrams or line charts with the median ± 95% confidence interval (CI) ($N \geq 3$, $n \geq 3$) for each group. The biological (N) and technical (n) replicated for each experiment are given in each figure.

3. Results

3.1. The stability of housekeeping genes in samples

When examining the expression of circadian rhythm genes in samples, it is essential to identify a housekeeping gene with stable expression. This housekeeping gene is used to normalize the expression of the circadian rhythm genes. Four housekeeping genes (RPL13a, EF1a, GAPDH, and B2M) were evaluated to assess their stability in the samples. The qRT-PCR data were analyzed using ΔCt, Bestkeeper, GeNorm, and NormFinder, along with the RefFinder tool (Xie et al., 2023). Based on the spider-web diagram in Figure 9, B2M is the most stable housekeeping gene in the samples.

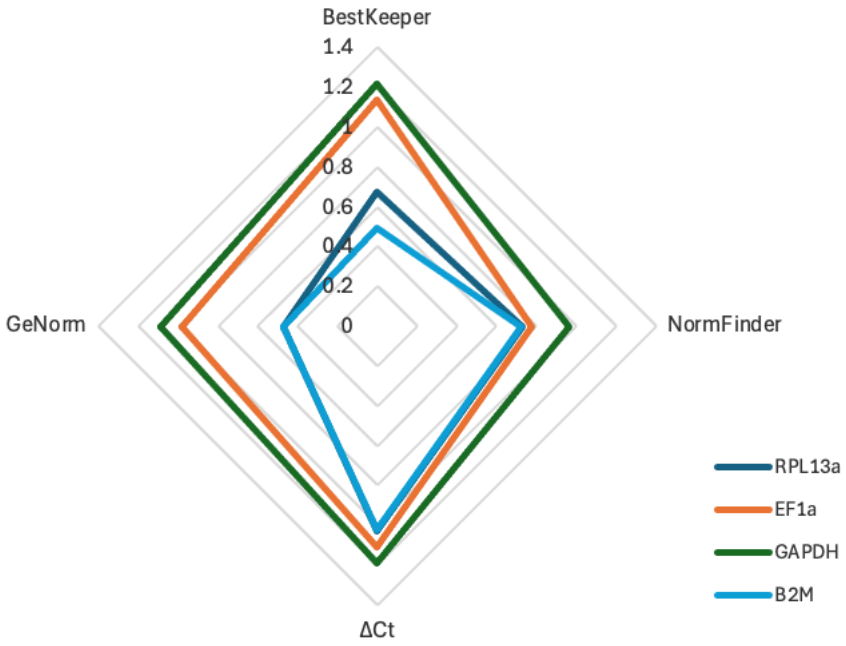

Figure 9 Stability of the four housekeeping genes in the samples

The expression of four housekeeping genes on day 21 in the 2D in vitro osteoblast-osteoclast co-culture model exposed to human serum or FCS was evaluated using quantitative real-time polymerase chain reaction (qRT-PCR). Four analytical methods (ΔCt, Bestkeeper, GeNorm, and NormFinder) along with the RefFinder tool were utilized to determine the stability of the housekeeping genes. A lower value indicates greater stability of the housekeeping gene. The data are presented as a spider-web diagram.

3.2. The circadian gene expression pattern in the *in vitro* co-culture model with FCS

We established an *in vitro* co-culture model of the osteoblast-osteoclast with FCS in a 6-well plate and tested its suitability to demonstrate the circadian rhythm. Following incubation for 21 days, we collected RNA at three time points: morning (7–8 am), afternoon (1–2 pm), and evening (7–8 pm). After synthesizing cDNA, we used qRT-PCR to detect the expression of circadian rhythm genes. CRY1 (Figure 10A), PER1 (Figure 10B), PER2 (Figure 10C), BMAL1 (Figure 10D), and NPAS2 (Figure 10F) demonstrated no peak in gene expression, whereas CLOCK (Figure 10E) showed a morning peak. We compared these results with what has been reported in the literatures. Specifically, BMAL1, CLOCK, and NPAS2 exhibited an evening peak; PER1 and PER2 exhibited a morning peak; and CRY1 exhibited an evening peak (Schilperoort et al., 2020; Zvonic et al., 2007). Our results differ from what has been reported. This difference in circadian rhythm gene expression can be attributed to the inability of the co-culture model containing FCS to demonstrate the circadian rhythm. Therefore, the use of FCS to illustrate circadian rhythm *in vitro* is not a valuable and reliable methodology.

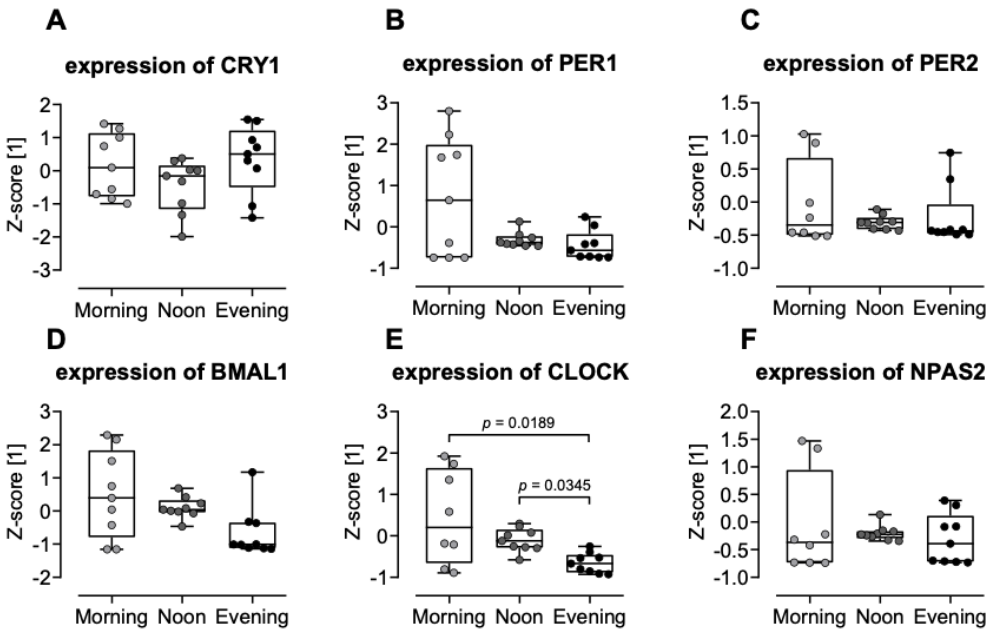

Figure 10 Circadian gene expression in the co-culture model with FCS

THP-1 and SCP-1 cells were co-cultured in a 6-well plate at a ratio of 8:1 in differentiation medium containing 2% FCS for 21 days. Then, RNA was collected in the morning (7–8 am), afternoon (1–

2 pm), or evening (7–8 pm) to examine the expression of six circadian rhythm genes: (A) CRY1, (B) PER1, (C) PER2, (D) BMAL1, (E) CLOCK, and (F) NPAS2. The data (N = 3, n = 3) are presented with bar diagrams. Statistical analysis: delta-delta Ct (ΔΔCt) algorithm, z-score [1], and the Kruskal–Wallis test.

3.3.1. The effects of different human serum concentrations on cell growth in the 2D *in vitro* co-culture model

We found that FCS could not effectively demonstrate the circadian rhythm in the *in vitro* osteoblast-osteoclast co-culture model. Hence, we replaced FCS with human serum. Initially, we compared the impact of two human serum concentrations: 1% and 2% on cell growth on days 7, 14, and 21 with the resazurin conversion assay and SRB staining. The addition of 2% human serum resulted in higher mitochondrial activity than 1% human serum on days 7 and 14. However, by day 21, the co-culture with 1% human serum exhibited higher mitochondrial activity than the co-culture with 2% human serum (Figure 11A). The co-culture with 1% human serum exhibited lower SRB staining compared with the co-culture with 2% at all time points (Figure 11B). Based on these results, the use of 2% human serum proved to demonstrate higher effectiveness in promoting cell growth than 1% human serum.

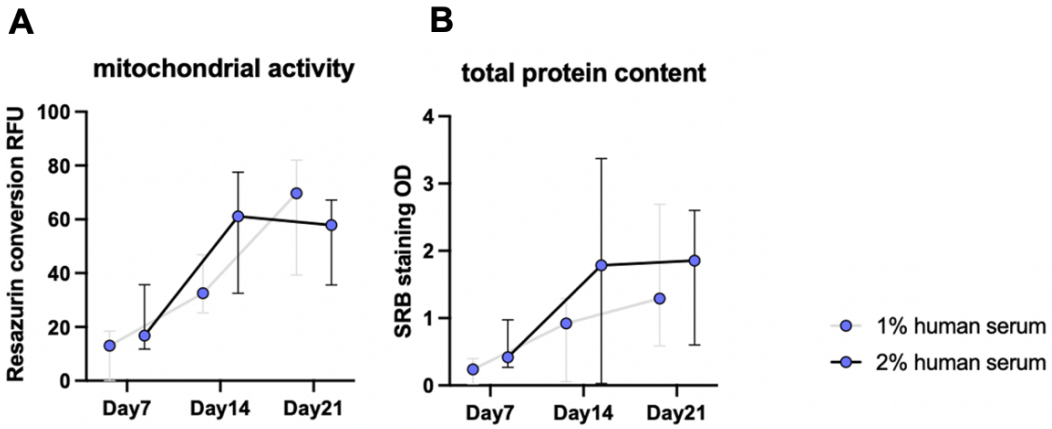

Figure 11 The growth of cells is promoted by the presence of human serum in the 2D co-culture model

The variation in effects caused by different concentrations of human serum on cell growth were examined. (A) Mitochondrial activity was assessed at 30, 60, 90, and 120 minutes after the addition of the resazurin working solution. (B) Cell growth was assessed by staining surface proteins with sulforhodamine B (SRB). On days 7, 14, and 21, the cells were fixed with 99%

alcohol at –20°C for at least 1 hour before analysis. The data (N = 3; n = 3) were compared and are presented as line charts with the median ± 95% confidence interval. Statistical analysis: non-parametric version of a two-way ANOVA.

3.3.2. The effects of different human serum concentrations on osteoblast and osteoclast function in the 2D *in vitro* co-culture model

Next, we examined the effect of 1% and 2% human serum on the activity of osteoblasts and osteoclasts by using the CA II, TRAP, and AP activity assays. Based on the CA II results, 1% human serum was less effective than 2% human serum in promoting the differentiation and function of osteoclasts in the co-culture on day 21, but it was more effective on days 7 and days 14. And no significant differences were observed in CA II activity between the co-cultures with 1% and 2% human serum on days 7, 14, and 21 (Figure 12A). Regarding TRAP, which indicates osteoclast function after maturation and differentiation, the co-culture with 2% human serum had higher activity than the co-culture with 1% human serum on days 7 and 21 (Figure 12B). However, on day 14, there was higher activity in the co-culture with the 1% human serum. Overall, TRAP activity did not differ significantly between the co-cultures with 1% and 2% human serum on days 7, 14, and 21. Finally, AP, which reflects osteoblast function, demonstrated consistently and slightly higher activity in the co-culture with 1% human serum at all three time points. Nevertheless, there was no statistically significant differences appeared between the co-cultures with 1% and 2% human serum on days 7, 14, and 21 (Figure 12C). These findings indicate that 1% human serum outperformed 2% human serum at all time points, making it suitable for use in the subsequent experiments.

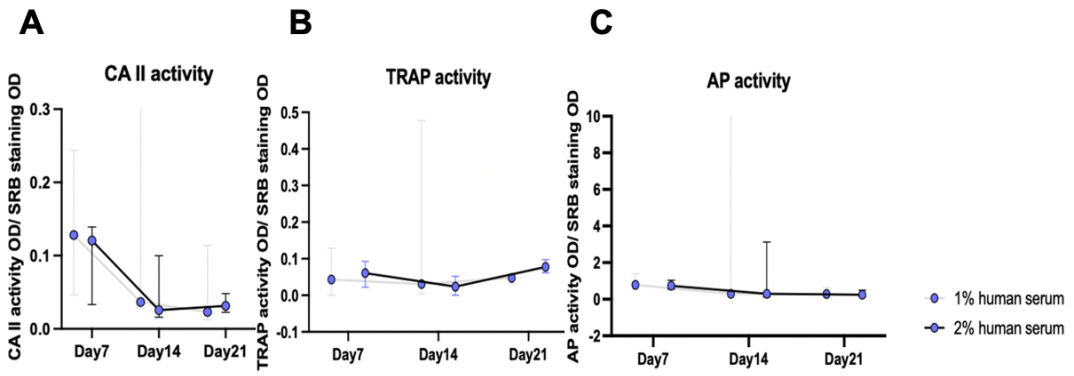

Figure 12 Osteoblast function and osteoclast differentiation and function

The 2D *in vitro* osteoblast-osteoclast co-culture model was cultured for 7, 14, or 21 days with 1% or 2% human serum, and osteoblast and osteoclast functions were assessed based on enzymatic activities. (A) Subsequent to a complete PBS wash, the CA II detection solvent was added to the wells, and the cells were analyzed immediately using a plate reader for 15 minutes. (B) The supernatant was collected and incubated with TRAP detection reagent for 6 hours before analysis. (C) Following a thorough wash with PBS, the AP detection reagent was added to the wells, and the cells were analyzed using a plate reader after 3 hours. The data (N = 3; n = 3) are presented as line charts with the median ± 95% confidence interval. Statistical analysis: non-parametric version of a two-way ANOVA.

3.4.1. The effects of 1% human serum collected at different times of the day on cell growth in the 2D *in vitro* co-culture model

We examined cell growth based on the resazurin conversion assay and SRB staining to determine differences in 1% human serum collected in the morning, noon, and evening on days 7, 14, and 21. At each time, there were no significant differences in resazurin conversion (Figure 13A) and SRB staining (Figure 13B). Of note, both factors increased over time. In summary, the time of day that human serum was collected did not alter cell growth parameters.

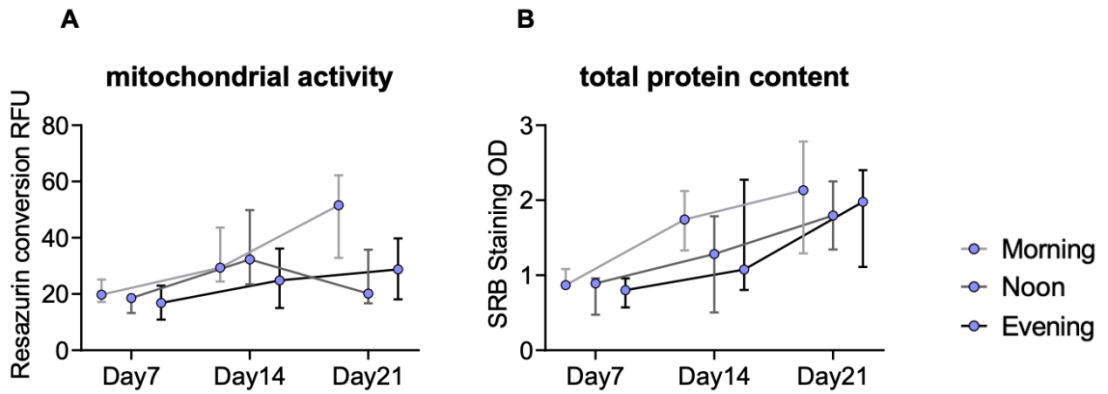

Figure 13 The impact of human serum collected at three times of the day on bone cell growth

Cell growth was assessed in the 2D *in vitro* osteoblast-osteoclast co-culture model exposed to 1% human serum (collected in the morning, afternoon, or evening) on days 7, 14, and 21. Resazurin conversion was used to assess mitochondrial activity, and SRB staining was used to stain cell-surface proteins. The data (N = 4; n = 3) are presented as line charts with the median ± 95% confidence interval. Statistical analysis: non-parametric version of a two-way ANOVA.

3.4.2. The expression of cell proliferation and growth genes in the *in vitro* 2D co-culture model

Next, we analyzed the expression of the genes related to cell proliferation and growth—MKI67, TOP2A, and TPX2—on day 21 in the 2D *in vitro* co-culture model with human serum collected in the morning, afternoon, or evening. MKI67, TOP2A, and TPX2 gene expression was highest in the co-culture with human serum collected in the evening (Figure 14). TOP2A and TPX2 gene expression was significantly higher in the co-culture with human serum collected in the evening compared with the co-culture with human serum collected in the afternoon (Figure 14B and 14C, respectively). MKI67, TOP2A, and TPX2 gene expression was lowest in the co-culture model with osteoblast and osteoclast with human serum collected in the afternoon, while the co-culture with human serum collected in the morning showing intermediate expression.

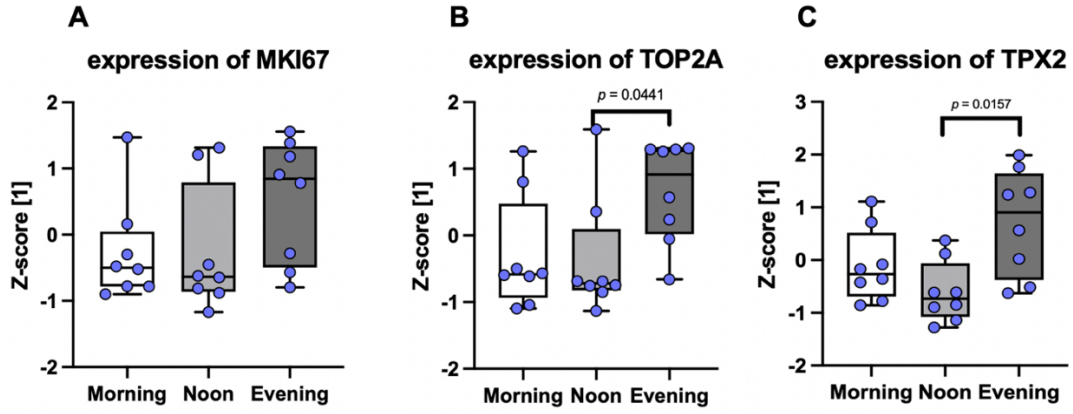

Figure 14 The effects of human serum collected in the morning, afternoon, and evening on the expression of genes related to cell proliferation and growth

The expression of cell proliferation and growth genes at day 21 in the 2D *in vitro* osteoblast-osteoclast co-culture model exposed to human serum collected in the morning, afternoon, or evening. The bar diagrams show the expression of the (A) MIK67, (B) TOP2A, and (C) TPX2 genes. Statistical analysis: the delta-delta Ct (ΔΔCt) algorithm, z-score [1], and Kruskal–Wallis test.

3.4.3. The effects of 1% human serum collected at different times of the day on osteoblast and osteoclast function in the 2D *in vitro* co-culture model

We assessed bone cell differentiation and function on day 21 in the *in vitro* co-culture model exposed to 1% human serum collected in the morning, afternoon, or evening. We selected this time point because most bone cells have completed differentiation and exhibit mature functions by this time. Based on CA II activity, the degree of osteoclast differentiation varied depending on when the human serum was collected, with the highest activity in the co-culture with human serum collected in the evening and the lowest in the co-culture with human serum collected in the morning (Figure 15A). Furthermore, TRAP activity demonstrated variable osteoclast function: It was highest in the co-culture with human serum collected in the morning, followed by the co-culture with human serum collected in the evening and morning (Figure 15B). Finally, the AP activity results revealed significant variations in osteoblast function between the co-cultures with human serum collected in the morning and evening, with the highest activity in the former and the lowest activity in the latter. The co-culture with human serum collected in the afternoon showed intermediate AP activity (Figure 15C).

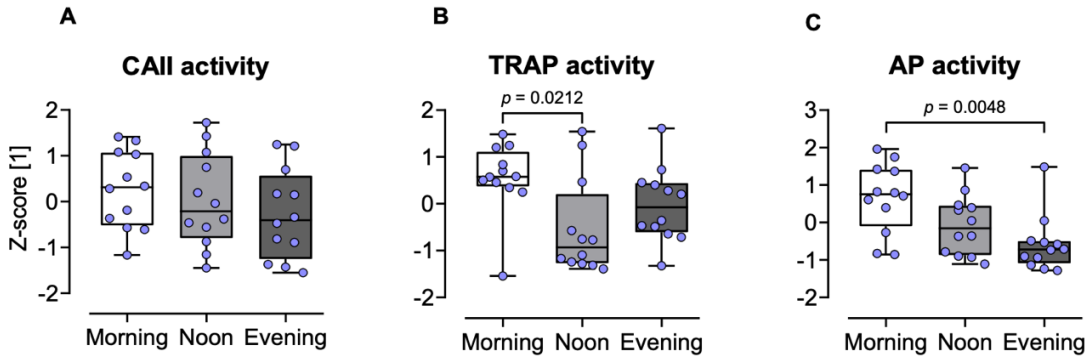

Figure 15 The effects of human serum collected in the morning, afternoon, and evening on osteoclast and osteoblast differentiation and function

Osteoblast and osteoclast function was examined on day 21 in the 2D *in vitro* osteoblast-osteoclast co-culture with 1% human serum collected in the morning, afternoon, or evening. (A) CA II activity was assessed as a marker of osteoclast differentiation. Then washed cells with PBS, incubated with the CA II detection reagent, and analyzed immediately with a plate reader for 15 minutes. (B) The supernatant was collected and incubated with TRAP detection reagent for 6 hours before analysis with a plate reader. (C) Following a thorough wash with PBS, the AP detection reagent was mixed into the wells, and the cells were analysed using a plate reader after 3 hours. The data (N = 4, n = 3) are presented with bar diagrams. Statistical analysis: z-score [1] and the Kruskal–Wallis test.

3.5. Differences in the formation of bone calcium matrix between the 2D and 3D co-culture models

We utilized Alizarin Red staining to visualize the extracellular calcium matrix on day 21 in the 2D co-culture model exposed to 1% human serum collected in the morning, afternoon, or evening. Based on this staining, the co-culture with human serum collected in the evening exhibited the highest calcium matrix content, while the co-culture with human serum collected in the morning displayed the lowest content (Figure 16B, the image of from 1 of 4 rounds). In the 3D co-culture model, with the THP-1 and SCP-1 cells seeded on PRP scaffolds and exposed to 1% human serum collected in the morning, afternoon, or evening, we used CT to determine mineral density and the ZwickLine machine to determine stiffness. CT indicated significant differences between the 3D co-cultures with human serum collected in the evening and morning and between the 3D co-cultures with human serum collected in the evening and afternoon, with the highest mineral density in

the co-culture with human serum collected in the evening (Figure 16C). The ZwickLine machine demonstrated significant differences in stiffness between the co-cultures with human serum collected in the evening and morning, with the former showing the highest stiffness (Figure 16D). Taken together, the Alizarin Red staining results from the 2D co-culture model are largely consistent with the CT and ZwickLine machine findings from the 3D co-culture model, with similar trends across both models.

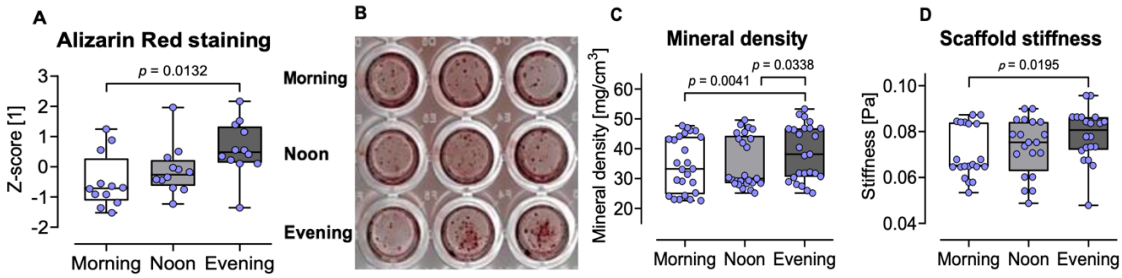

Figure 16 Analysis of the extracellular calcium matrix in in the 2D and 3D *in vitro* models
The formation of a bone calcium matrix on day 21 was assessed in the 2D and 3D *in vitro* osteoblast-osteoclast co-culture models with 1% human serum collected in the morning, afternoon, or evening. (A) Alizarin Red staining was employed to evaluate the calcium matrix generated by osteoblasts in the 2D *in vitro* co-culture model. The data (N = 4, n = 3) are presented with a bar diagram. (B) A representative image from 1 of 4 rounds of Alizarin Red staining. In the 3D *in vitro* co-culture model, (C) CT was used to determine mineral density. The data (N = 5; n = 15) are presented with a bar diagram. In addition, the (D) ZwickLine machine was used to measure the stiffness of the platelet-rich plasma scaffolds. The data (N = 5, n = 4) are presented with a bar diagram. Statistical analysis: z-score [1] and the Kruskal–Wallis test.

3.6. The expression of circadian rhythm genes in the 2D *in vitro* co-culture model

Finally, we used qRT-PCR to assess the expression of the circadian genes CLOCK, BMAL1, NPAS2, CRY1, PER1, and PER2 on day 21 in the 2D co-culture model with 1% human serum collected in the morning, afternoon, or evening. CRY1 expression was highest in the co-culture with human serum collected in the morning (Figure 17A), while CLOCK, BMAL1, and NPAS2 reached their highest expression in the co-culture with human serum collected in the afternoon (Figure 17E, 17D, and 17F, respectively). PER1 and PER2 exhibited peak

expression in the co-culture with human serum collected in the evening (Figure 17B and 17C, respectively). These findings are largely consistent with the gene expression patterns reported for mouse skull tissue. Specifically, BMAL1, CLOCK, and NPAS2 exhibited an evening peak; PER1 and PER2 exhibited a morning peak; and CRY1 exhibited an evening peak (Schilperoort et al., 2020; Zvonic et al., 2007). Based on the collected data, the *in vitro* circadian rhythm co-culture model of the osteoblasts and osteoclasts, constructed by replacing FCS with human serum collected at different times of the day serves as a reliable representation of the circadian rhythm.

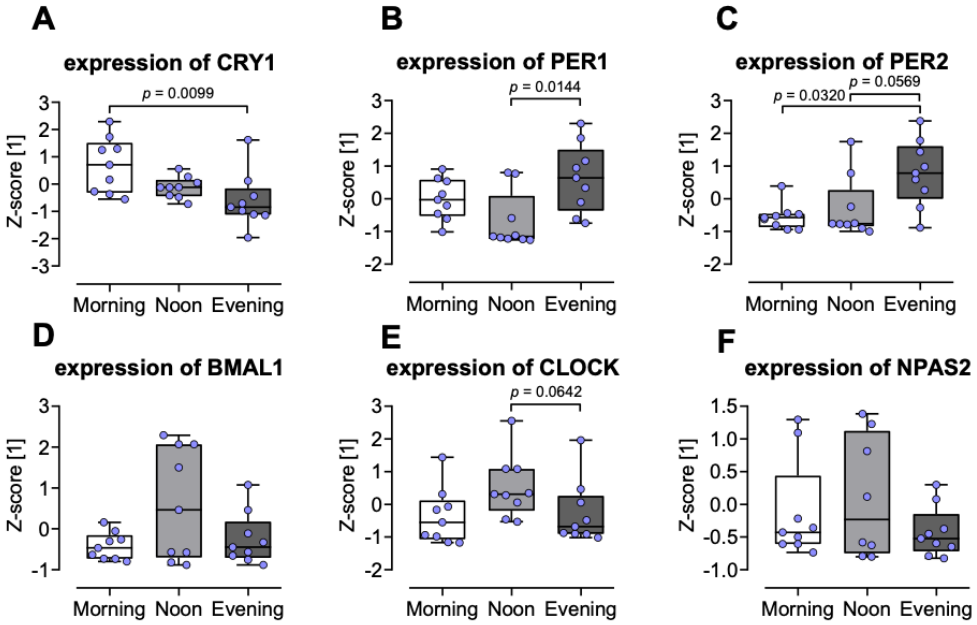

Figure 17 The expression of circadian rhythm genes in the 2D co-culture model

The expression of the following circadian rhythm genes was tested on day 21 in the 2D *in vitro* osteoblast-osteoclast co-culture model with 1% human serum collected in the morning, afternoon, or evening: (A) CRY1, (B) PER1, (C) PER2, (D) BMAL1, (E) CLOCK, and (F) NPAS2. The data (N = 3, n = 3) are presented with bar diagrams. Statistical analysis: the delta-delta Ct (ΔΔCt) algorithm, z-score [1], and Kruskal–Wallis test.

4. Discussion

4.1. The use of FCS in the *in vitro* co-culture model could not demonstrate the circadian rhythm

The term “circadian rhythm” refers to a natural oscillatory process in the human body that operates on a 24-hour cycle, influenced by changes in external light intensity throughout the day (Patke et al., 2020). The eyes transmit the perceived light changes to the SCN (Hastings et al., 2018), which releases substances into the blood to synchronize the circadian rhythm of other tissues and cells to the central circadian rhythm (Akashi & Nishida, 2000; Balsalobre et al., 1998). Of note, the SCN is missing in the *in vitro* cell culture model, and prior experiments have shown that circadian rhythms in *in vitro* cell models also need to be synchronized with the central circadian rhythm (Landgraf et al., 2014). In previous studies, researchers have used hepatocytes and fibroblasts to construct an *in vitro* circadian rhythm model and put forward the idea that synchronization is an essential point in demonstrating circadian rhythms, with serum identified as the key point of synchronization (Dibner et al., 2010; Francia et al., 2024; Niehoff et al., 2021). For this reason, we initially tested whether FCS could be used to demonstrate the circadian rhythm in the *in vitro* osteoblast-osteoclast co-culture model.

The initial results with the 2D co-culture model with FCS demonstrated expression changes in genes linked to the circadian rhythm did not show the expected changes throughout the day, the CRY1, PER1, PER2, BMAL1, and NPAS2 demonstrated no peak in gene expression, whereas CLOCK showed a morning peak. These findings differ from what has been reported in the literature: CLOCK, BMAL1, and NPAS2 usually show peak gene expression between the morning and afternoon; PER1 and PER2 showed the expression peaks between the afternoon and evening; and CRY1 expression peaks in the early morning (Schilperoort et al., 2020). Our disparate results showed that FCS is unable to synchronize the circadian rhythm in tissues and cells with the central circadian rhythm. Therefore, it is not suitable for use in an *in vitro* osteoblast-osteoclast co-culture model to display the circadian rhythm and must be replaced.

4.2. Determination of the optimal human serum concentration to replace FCS

We considered the use of human serum collected at different time points, consistent with a previous study (Kasukawa et al., 2012), to replace FCS in the *in vitro* osteoblast-osteoclast co-culture model. In brief, we collected blood from 10 healthy volunteers in the morning (7–8 am), afternoon (1–2 pm), and evening (7–8 pm). We centrifuged the blood to obtain serum (approximately 3 mL per sample) and stored it at –80°C (Grankvist et al., 2019).

After we obtained the serum, we wondered which concentration should be utilized in the *in vitro* osteoblast-osteoclast co-culture model to show the human circadian rhythm. Ultimately, we tested four concentrations: 1%, 2%, 3%, and 4% (Ferro et al., 2012). Some studies have demonstrated that mammalian serum contains a considerable quantity of cell growth factors, protein amino acids, and a variety of nutrients that facilitate cell growth (Montali et al., 2016). The 3% and 4% human concentrations have a greater quantity of nutrients and could allow cells to proliferate at a faster rate than in the presence of 1% and 2% human serum (Liljander et al., 2011). Based on resazurin conversion and SRB staining (McMillian et al., 2002; Skehan et al., 1990), after 7, 14, and 21 days, the use of 3% or 4% human serum led to cell detachment. Hence, we deduced that 3% and 4% human serum may not allow sufficient time for the cells to complete differentiation because the presence of elevated nutrient concentrations accelerates cell growth. For the other two concentrations, the presence of 2% human serum led to faster cellular growth compared with the use of 1% serum.

We also assessed the effects of 1% and 2% human serum on the CA II, TRAP and AP activities to assess osteoclast differentiation, osteoclast function, and osteoblast function, respectively(Bernhardt et al., 2017; Ehnert et al., 2010; Minkin, 1982). We examined these activities at 7, 14, and 21 days. Based on our results, 2% human serum exerted a greater impact on the differentiation of osteoclast. For osteoclast function, however, the 1% concentration was more

efficacious than the 2% concentration. Finally, osteoblast function was higher in the presence of 1% human serum. Considering cell growth and these activities, we chose to use 1% human serum in our cell model of co-culture for the subsequent experiments.

4.3. The circadian rhythm in the *in vitro* co-culture model with human serum collected in the morning, afternoon, and evening

4.3.1. Osteoblast and osteoclast growth in the 2D co-culture

After establishing the optimal human serum concentration, we assessed osteoblast and osteoclast growth at 7, 14, and 21 says in the 2D co-culture model. We examined differences when using human serum collected in the morning, afternoon, or evening. Based on resazurin conversion and SRB staining, cell growth did not differ depending on when the human serum was collected. Previous studies have not indicated that the proliferation of human bone cells is regulated by the circadian rhythm *in vitro*. Therefore, the circadian rhythm has no apparent significant impact on osteoblast and osteoclast growth.

We also determined gene expression at 21 days by using qRT-PCR. We examined three genes related to cell growth and division: MKI67, TOP2A, and TPX2 (Matson et al., 2021; Nakagawa et al., 2011; Sahin et al., 2016). The expression of these genes did not differ depending on when the human serum was collected, consistent with the resazurin conversion and SRB staining results.

4.3.2. Osteoblast and osteoclast differentiation and function in the 2D co-culture

We also examined CA II, TRAP, and AP activities and performed Alizarin Red staining on day 21 for the 2D *in vitro* osteoblast-osteoclast co-culture model. CA II activity did not differ depending on when the human serum was collected. However, TRAP activity showed differences. Specifically, it was highest in the co-culture with the morning human serum; the activity in this co-culture differed

significantly compared with the co-culture with human serum collected in the afternoon. The co-culture with human serum collected in the evening showed intermediate TRAP activity. A potential explanation for these differences is that serum contains varying concentrations of cytokines that influence osteoclast differentiation and function, including RANKL, M-CSF, IL-6, and Transforming Growth Factor Beta (TGF-β), among others (Kawamoto et al., 2016; Li et al., 2010). This discrepancy is manifested in the concentration and variety of cytokines present in the morning, noon, and evening (Diemar et al., 2023). AP activity displayed notable differences between the co-cultures treated with human serum collected in the morning and evening, with the co-culture with human serum collected in the afternoon showing intermediate AP activity. The serum levels of BMP, TGF-β, IGF-1, and Vascular Endothelial Growth Factor (VEGF), among other factors, may be responsible for the differences in AP activity. Cytokines exert specific effect on the function of osteoclasts and osteoblasts (Liu et al., 2012; Rico-Llanos et al., 2017; Wu et al., 2016). The serum levels of these factors fluctuate regularly over a 24-hour period, thus showing a circadian rhythm (Crosby et al., 2019; Dong et al., 2016; Ze et al., 2025).

In our 2D *in vitro* osteoblast-osteoclast co-culture cell model, the osteoblasts are responsible for producing the extracellular calcium matrix (Hadjidakis & Androulakis, 2006). Conversely, the osteoclasts are responsible for the processes of absorbing and dissolving the calcium matrix (Veis & O'Brien, 2023). Given that osteoblasts and osteoclasts typically undergo simultaneous growth, bone formation and resorption frequently occur concurrently. A straightforward approach to assess bone formation and resorption is to determine the amount of calcium in the extracellular matrix (Lutter et al., 2010). To this end, we employed Alizarin Red staining to determine the calcium matrix content in the co-culture model (Bernar et al., 2022). The calcium matrix content was the highest in the co-culture with human serum collected in the evening and lowest in the co-culture with human serum collected in the morning; the difference between these co-cultures was significant. These findings suggest that the circadian rhythm effect on the extracellular calcium matrix is influenced by the combined effects of bone

formation and resorption, a finding consistent with the previously documented effects of the circadian rhythm on osteoblast and osteoclast functions.

4.3.3. Osteoblast and osteoclast differentiation and function in the 3D co-culture

For the 3D *in vitro* osteoblast-osteoclast co-culture model, we used CT to assess the calcium matrix density. We found that it was highest in the co-culture with human serum collected in the evening, followed by the co-cultures with human serum collected in the afternoon and morning. Of note, the density of the co-culture with human serum collected in evening differed significantly compared with the co-cultures with human serum collected in the afternoon and morning. The observations are compatible with the Alizarin Red staining of the 2D co-culture model.

We also used the ZwickLine machine to assess matrix stiffness. Consistent with the CT imaging, the co-culture with human serum collected in the evening had the stiffest matrix, followed by the co-cultures with human serum collected in the afternoon and morning. A statistically significant difference was found between the co-culture with human serum collected in the evening and the co-culture with human serum collected in the morning. This indicates that human osteoblasts are most active in the morning, and osteoblast activity is higher than osteoclast activity in the morning, which allows them to accumulate a large amount of calcium extracellular matrix. We postulate that the discrepancies in outcomes across different time points between the 2D and 3D co-culture models are consequence of the variations in osteoblast and osteoclast function at different times. These discrepancies in outcomes mirror the circadian rhythm of osteoblast and osteoclast activity.

4.4. Evaluation of the reliability of the *in vitro* co-culture model to represent the circadian rhythm

We successfully demonstrated the circadian rhythm of osteoblast and osteoclast of human using human serum in a new *in vitro* osteoblast-osteoclast co-culture model. At present, there is no available research on related circadian rhythm of human being cell models to serve as a reference, consequently, reliability cannot be easily ascertained in our new *in vitro* co-culture model. Nevertheless, researchers have reported the expression pattern of circadian genes in human liver tissue, adipose tissue, and bone tissue from animal models (Kiehn et al., 2017; Reinke & Asher, 2016; Zvonic et al., 2007). These studies showed consistent circadian gene expression patterns and thus can be used as a reference.

We found that BMAL1, NPAS2, and CLOCK exhibited peak gene expression in the co-culture with human serum collected in the afternoon; CRY1 demonstrated peak gene expression in the co-culture model with human serum collected in the morning; and PER1 and PER2 exhibited peak gene expression in the co-culture model with human serum collected in the evening. These findings align with those reported previously for mouse calvaria (Schilperoort et al., 2020; Zvonic et al., 2007). The consistent circadian gene expression pattern in our *in vitro* osteoblast-osteoclast co-culture model with human serum relative to the findings from prior research substantiate our model's reliability.

4.5. Limitations

We successfully established a human *in vitro* osteoblast-osteoclast co-culture cell model and demonstrated that is reliably replicates the circadian rhythm. Nevertheless, further improvements are necessary to address some limitations. First, our model requires human serum to facilitate cell differentiation and circadian rhythm synchronization. Hence, a sufficient quantity of human serum collected at specific times must be obtained to maintain the integrity of the model. In addition, the volunteers must be healthy. These conditions undoubtedly

present challenges for this model. Second, we considered three times points–morning (7–8 am), noon (1–2 pm), and evening (7–8 pm)—with a 6-hour interval between each period. However, the authors of another study collected experimental samples from animals every 4 hours for a period of 48 hours (Zvonic et al., 2007). A shorter interval before serum collection can be expected to more accurately represent the dynamic changes in cell function brought about by the circadian rhythm. It would be beneficial to reduce the time interval for the collection of human serum and to extend the time period for the collection of serum samples, but this would undoubtedly increase the difficulty in recruiting subjects. Finally, we aimed to demonstrate the circadian rhythm in our model, and the impact of certain illnesses on the circadian rhythm remains largely unexplored, with diabetes being a notable example. Subsequent experiments will allow for the investigation of the relationship between certain diseases and circadian rhythm disorders, thereby facilitating a more profound comprehension of the circadian rhythm.

4.6. Outlook

Currently, research on circadian rhythm–related diseases is primarily conducted through animal experimentation, with a focus on certain cell-related factors in human blood (Neves et al., 2022). However, these research methods are constrained by the limitations of the research platform and are unable to allow direct observation of the effects of diseases on the morphology, function, and growth of cells. For example, research on the relationship between type 2 diabetes and the circadian rhythm is currently primarily conducted through animal experimentation and the examination of blood samples from individuals with diabetes (Javeed & Matveyenko, 2018). Our new cell model offers a convenient platform for directly observing the impact of diabetes on cellular differentiation, growth, and function, as well as the regulatory effect of circadian rhythm in cells.

Furthermore, the abundance of cell types and their accessibility, in comparison to animal experiments, mean that our co-culture model is more cost-effective and

has fewer ethical constraints. The utilization of diverse cellular types allows for the construction of various cell models, which is capable of being used to examine the effect of the circadian rhythm on disparate cellular entities. For example, the construction of a cell model using bone cells allows for the researching the circadian rhythm expression in bone cells, In the process of constructing the cell model Applying liver cells makes it possible to investigate the circadian rhythm in liver cells. This approach facilitates a more profound comprehension of the functions and consequences of rhythmic activity in a range of tissue cells, including those in diseased conditions.

4.7. Conclusion

We first sought to demonstrate the circadian rhythm in an *in vitro* osteoblast-osteoclast co-culture model using FCS. To this end, analyzed the expression of CLOCK, BMAL1, NPAS2, CRY1, PER1, and PER2—genes related to the circadian rhythm—after collecting cells in the morning (7–8 am), afternoon (1–2 pm), and evening (7–8 pm). The peak expression of these genes differed from what has been reported in the literature, indicating that FCS cannot be used to develop an *in vitro* osteoblast-osteoclast co-culture model to demonstrate the circadian rhythm. Therefore, it was necessary to identify an alternative to FCS to demonstrate the circadian rhythm *in vitro*. Given that serum plays a pivotal role in the synchronization of circadian rhythms within tissues and cells, we investigated the potential of human serum as an alternative to FCS.

We procured blood samples from healthy young volunteers at three times, namely morning, afternoon, and evening, on the same day, and then separated serum from these samples. First, we established that a 1% human serum concentration was an appropriate substitute for 2% FCS in the cell model. Then, we examined the effects of 1% human serum collected in the morning, afternoon, and evening on osteoblast and osteoclast growth and function. We also assessed a 3D model by seeding the cells on PRP scaffolds, to provide a better model of *in vivo* bone. The 2D and 3D co-culture models successfully demonstrated the circadian rhythm of osteoblasts and osteoclasts, confirming the reliability of our

in vitro cell model for circadian rhythm studies. Our *in vitro* model closely replicates *in vivo* conditions, capturing the temporal aspects of bone metabolism that are otherwise challenging to observe.

In conclusion, our novel *in vitro* osteoblast-osteoclast co-culture system offers excellent programmability and a reliable platform for further investigation concerning the influence of circadian rhythms on bone metabolism. This model could be used to examine the potential contribution of a disrupted circadian rhythm to bone disorders. A platform like this could potentially also prove invaluable in the development and testing of therapeutic strategies that are dependent on time, with the aim of optimizing therapeutic effectiveness Via timing interventions to match the body's intrinsic circadian rhythm.

5.1. Summary

It is widely accepted that the circadian rhythm regulates the metabolism and functions of osteoblasts and osteoclasts. Existing research on the circadian rhythm of osteocytes has primarily focused on human blood tissues and animal models. However, the limitations of using bone conversion factors in these models prevent the development of a simple, direct, and reliable method for observing how circadian rhythms influence osteoblast and osteoclast activity. To address this gap, we successfully established an *in vitro* osteoblast-osteoclast co-culture model to demonstrate circadian rhythmicity. This model incorporates 1% human serum collected at three different times of the day—morning, afternoon, and evening (Figure 18).

Our *in vitro* osteoblast-osteoclast co-culture model synchronizes the central circadian rhythm, originating from the suprachiasmatic nucleus (SCN), with the circadian rhythms of osteoblasts and osteoclasts through the use of 1% human serum. After 21 days of culture, osteoblast and osteoclast functional activities exhibited distinct circadian patterns, characterized by regular fluctuations across morning, afternoon, and evening periods. Both cell types showed peak activity levels in the morning, followed by a gradual decline. Notably, osteoblast activity was lowest in the evening, whereas osteoclast activity reached its nadir in the afternoon.

To validate the reliability of this newly developed circadian rhythm cell model, we analyzed the expression profiles of key circadian rhythm-related genes (BMAL1, CLOCK, NPAS2, PER1, PER2, CRY1). The observed gene expression patterns were compared to previously reported circadian gene expression data in the literature. The high degree of similarity between the two datasets supports the validity of our *in vitro* co-culture model for investigating the circadian behavior of osteoblasts and osteoclasts

We propose that our co-culture model represents a novel and valuable platform for studying circadian rhythms, providing new opportunities to examine how

circadian disruptions affect osteoblast and osteoclast function. This model may contribute to a deeper understanding of the mechanisms underlying the increased fracture risk observed in individuals exposed to prolonged night shift work, as well as in patients with circadian rhythm-associated disorders.

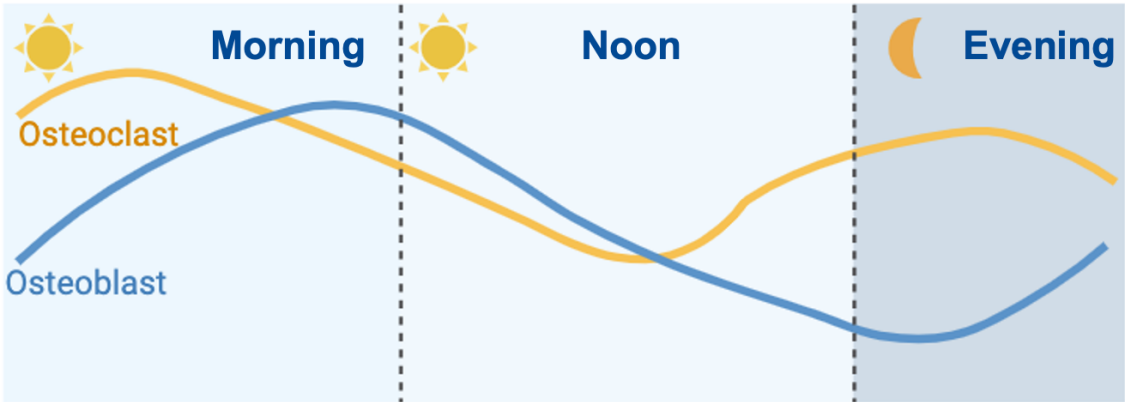

Figure 18 The circadian rhythm of osteoblasts and osteoclasts

Osteoclast activity exhibits a diurnal pattern, reaching maximum levels during the morning and minimum levels in the afternoon. In contrast, osteoblast activity shows the opposite pattern, exhibiting maximum levels in the morning and minimum levels in the evening. The image was generated through the use of Biorender (https://app.biorender.com/).

5.2. Zusammenfassung

Es ist allgemein anerkannt, dass der zirkadiane Rhythmus den Stoffwechsel sowie die Funktionen von Osteoblasten und Osteoklasten reguliert. Bisherige Forschungen zum zirkadianen Rhythmus von Osteozyten konzentrierten sich hauptsächlich auf menschliche Blutgewebe und Tiermodelle. Die Verwendung von Knochenumbaumarkern in diesen Modellen ist jedoch mit Einschränkungen verbunden, die die Entwicklung einer einfachen, direkten und zuverlässigen Methode zur Beobachtung der Auswirkungen des zirkadianen Rhythmus auf die Aktivität von Osteoblasten und Osteoklasten erschweren. Um diese Lücke zu schließen, haben wir erfolgreich ein *in-vitro*-Kokulturmodell von Osteoblasten und Osteoklasten etabliert, das zirkadiane Rhythmen demonstriert. Dieses Modell verwendet 1 % menschliches Serum, das zu drei verschiedenen Tageszeiten – morgens, nachmittags und abends – gewonnen wurde (Abbildung 19).

Unser *in-vitro*-Kokulturmodell von Osteoblasten und Osteoklasten synchronisiert den zentralen zirkadianen Rhythmus, der vom suprachiasmatischen Nucleus (SCN) ausgeht, mit den zirkadianen Rhythmen der Osteoblasten und Osteoklasten durch die Zugabe von 1 % menschlichem Serum. Nach 21 Tagen Kultivierung zeigten die funktionellen Aktivitäten von Osteoblasten und Osteoklasten ausgeprägte zirkadiane Muster, die sich durch regelmäßige Schwankungen über die Tageszeiten hinweg – morgens, nachmittags und abends – charakterisieren ließen. Beide Zelltypen erreichten ihre höchste Aktivität am Morgen, gefolgt von einem allmählichen Rückgang. Bemerkenswerterweise war die Aktivität der Osteoblasten am Abend am geringsten, während die der Osteoklasten ihren Tiefpunkt am Nachmittag erreichte.

Zur Validierung der Zuverlässigkeit dieses neu entwickelten Zellmodells mit zirkadianem Rhythmus analysierten wir die Expressionsprofile zentraler zirkadianer Gene (BMAL1, CLOCK, NPAS2, PER1, PER2, CRY1). Die beobachteten Expressionsmuster wurden mit bereits veröffentlichten Daten zur Genexpression zirkadianer Gene verglichen. Die hohe Übereinstimmung

zwischen den beiden Datensätzen bestätigt die Validität unseres *in-vitro*-Kokulturmodells zur Untersuchung des zirkadianen Verhaltens von Osteoblasten und Osteoklasten.

Wir vertreten die Auffassung, dass unser Kokulturmodell eine neuartige und wertvolle Plattform zur Erforschung zirkadianer Rhythmen darstellt. Es bietet neue Möglichkeiten zur Untersuchung der Auswirkungen von Störungen des zirkadianen Rhythmus auf die Funktion von Osteoblasten und Osteoklasten. Dieses Modell könnte zu einem besseren Verständnis der Mechanismen beitragen, die dem erhöhten Frakturrisiko bei Personen mit langfristiger Nachtarbeit sowie bei Patienten mit zirkadianen Rhythmusstörungen zugrunde liegen.

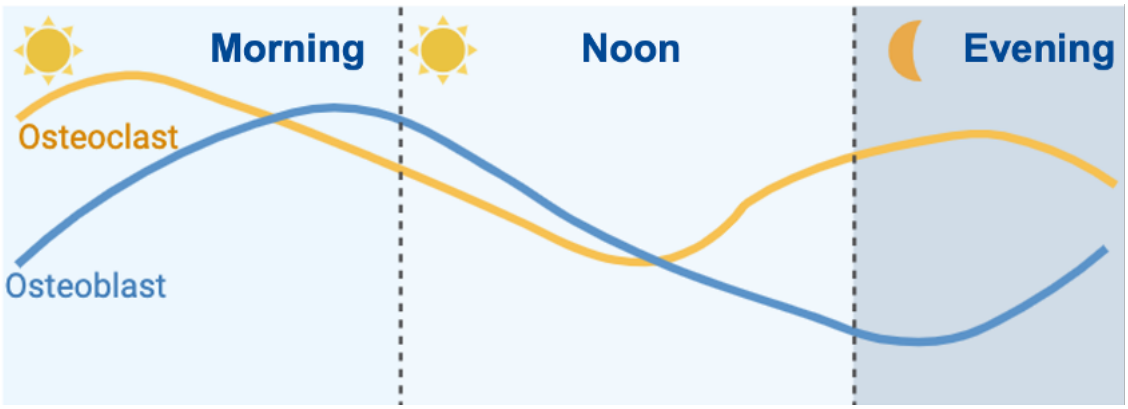

Abbildung 19 Der zirkadiane Rhythmus von Osteoblasten und Osteoklasten

Die Aktivität der Osteoklasten zeigt ein tageszeitliches Muster, mit den höchsten Werten am Morgen und den niedrigsten Werten am Nachmittag. Im Gegensatz dazu zeigt die Aktivität der Osteoblasten ein entgegengesetztes Muster, mit den höchsten Werten am Morgen und den niedrigsten am Abend. Das Bild wurde mit Unterstützung von BioRender erstellt (https://app.biorender.com/).

6. Bibliography

Akashi, M., & Nishida, E. (2000). Involvement of the MAP kinase cascade in resetting of the mammalian circadian clock. *Genes Dev*, *14*(6), 645-649. https://www.ncbi.nlm.nih.gov/pubmed/10733524

Aspera-Werz, R. H., Muck, J., Linnemann, C., Herbst, M., Ihle, C., Histing, T., Nussler, A. K., & Ehnert, S. (2022). Nicotine and Cotinine Induce Neutrophil Extracellular Trap Formation-Potential Risk for Impaired Wound Healing in Smokers. *Antioxidants (Basel)*, *11*(12). https://doi.org/10.3390/antiox11122424

Balsalobre, A., Damiola, F., & Schibler, U. (1998). A serum shock induces circadian gene expression in mammalian tissue culture cells. *Cell*, *93*(6), 929-937. https://doi.org/10.1016/s0092-8674(00)81199-x

Bar-Shavit, Z. (2007). The osteoclast: a multinucleated, hematopoietic-origin, bone-resorbing osteoimmune cell. *J Cell Biochem*, *102*(5), 1130-1139. https://doi.org/10.1002/jcb.21553

Bargiello, T. A., Jackson, F. R., & Young, M. W. (1984). Restoration of circadian behavioural rhythms by gene transfer in Drosophila. *Nature*, *312*(5996), 752-754. https://doi.org/10.1038/312752a0

Bernar, A., Gebetsberger, J. V., Bauer, M., Streif, W., & Schirmer, M. (2022). Optimization of the Alizarin Red S Assay by Enhancing Mineralization of Osteoblasts. *Int J Mol Sci*, *24*(1). https://doi.org/10.3390/ijms24010723

Bernhardt, A., Koperski, K., Schumacher, M., & Gelinsky, M. (2017). Relevance of osteoclast-specific enzyme activities in cell-based in vitro resorption assays. *Eur Cell Mater*, *33*, 28-42. https://doi.org/10.22203/eCM.v033a03

Blair, H. C. (1998). How the osteoclast degrades bone. *Bioessays*, *20*(10), 837-846. https://doi.org/10.1002/(SICI)1521-1878(199810)20:10<837::AID-BIES9>3.0.CO;2-D

Bocker, W., Yin, Z., Drosse, I., Haasters, F., Rossmann, O., Wierer, M., Popov, C., Locher, M., Mutschler, W., Docheva, D., & Schieker, M. (2008). Introducing a single-cell-derived human mesenchymal stem cell line expressing hTERT after lentiviral gene transfer. *J Cell Mol Med*, *12*(4), 1347-1359. https://doi.org/10.1111/j.1582-4934.2008.00299.x

Boivin, D. B., Boudreau, P., & Kosmadopoulos, A. (2022). Disturbance of the Circadian System in Shift Work and Its Health Impact. *J Biol Rhythms*, *37*(1), 3-28. https://doi.org/10.1177/07487304211064218

Bouchard, A. L., Dsouza, C., Julien, C., Rummler, M., Gaumond, M. H., Cermakian, N., & Willie, B. M. (2022). Bone adaptation to mechanical loading in mice is affected by circadian rhythms. *Bone*, *154*, 116218. https://doi.org/10.1016/j.bone.2021.116218

Boyce, B. F. (2013). Advances in the regulation of osteoclasts and osteoclast functions. *J Dent Res*, *92*(10), 860-867. https://doi.org/10.1177/0022034513500306

Bukowska-Damska, A., Skowronska-Jozwiak, E., Kaluzny, P., & Lewinski, A. (2022). Night shift work and osteoporosis - bone turnover markers among female blue-collar workers in Poland. *Chronobiol Int*, *39*(6), 818-825. https://doi.org/10.1080/07420528.2022.2037626

Bukowska-Damska, A., Skowronska-Jozwiak, E., Kaluzny, P., Lewinski, A., & Peplonska, B. (2020). Night shift work and osteoporosis among female blue-collar workers in Poland - a pilot study. *Chronobiol Int*, *37*(6), 910-920. https://doi.org/10.1080/07420528.2020.1763381

Burstone, M. S. (1959). Histochemical demonstration of acid phosphatase activity in osteoclasts. *J Histochem Cytochem*, *7*(1), 39-41. https://doi.org/10.1177/7.1.39

Chellappa, S. L., Vujovic, N., Williams, J. S., & Scheer, F. (2019). Impact of Circadian Disruption on Cardiovascular Function and Disease. *Trends Endocrinol Metab*, *30*(10), 767-779. https://doi.org/10.1016/j.tem.2019.07.008

Crosby, P., Hamnett, R., Putker, M., Hoyle, N. P., Reed, M., Karam, C. J., Maywood, E. S., Stangherlin, A., Chesham, J. E., Hayter, E. A., Rosenbrier-Ribeiro, L., Newham, P., Clevers, H., Bechtold, D. A., & O'Neill, J. S. (2019). Insulin/IGF-1 Drives PERIOD Synthesis to Entrain Circadian Rhythms with Feeding Time. *Cell*, *177*(4), 896-909 e820. https://doi.org/10.1016/j.cell.2019.02.017

Dibner, C., Schibler, U., & Albrecht, U. (2010). The mammalian circadian timing system: organization and coordination of central and peripheral clocks. *Annu Rev Physiol*, *72*, 517-549. https://doi.org/10.1146/annurev-physiol-021909-135821

Diemar, S. S., Dahl, S. S., West, A. S., Simonsen, S. A., Iversen, H. K., & Jorgensen, N. R. (2023). A Systematic Review of the Circadian Rhythm of Bone Markers in Blood. *Calcif Tissue Int*, *112*(2), 126-147. https://doi.org/10.1007/s00223-022-00965-1

Dong, C., Gongora, R., Sosulski, M. L., Luo, F., & Sanchez, C. G. (2016). Regulation of transforming growth factor-beta1 (TGF-beta1)-induced pro-fibrotic activities by circadian clock gene BMAL1. *Respir Res*, *17*, 4. https://doi.org/10.1186/s12931-016-0320-0

Ehnert, S., Baur, J., Schmitt, A., Neumaier, M., Lucke, M., Dooley, S., Vester, H., Wildemann, B., Stockle, U., & Nussler, A. K. (2010). TGF-beta1 as possible link between loss of bone mineral density and chronic inflammation. *PLoS One*, *5*(11), e14073. https://doi.org/10.1371/journal.pone.0014073

Ehnert, S., Rinderknecht, H., Aspera-Werz, R. H., Haussling, V., & Nussler, A. K. (2020). Use of in vitro bone models to screen for altered bone metabolism, osteopathies, and fracture healing: challenges of complex models. *Arch Toxicol*, *94*(12), 3937-3958. https://doi.org/10.1007/s00204-020-02906-z

Ferro, F., Spelat, R., Beltrami, A. P., Cesselli, D., & Curcio, F. (2012). Isolation and characterization of human dental pulp derived stem cells by using media containing low human serum percentage as clinical grade substitutes for bovine serum. *PLoS One*, *7*(11), e48945. https://doi.org/10.1371/journal.pone.0048945

Francia, M., Bot, M., Boltz, T., De la Hoz, J. F., Boks, M., Kahn, R. S., & Ophoff, R. A. (2024). Fibroblasts as an in vitro model of circadian genetic and genomic studies. *Mamm Genome*, *35*(3), 432-444. https://doi.org/10.1007/s00335-024-10050-7

Grankvist, K., Gomez, R., Nybo, M., Lima-Oliveira, G., & von Meyer, A. (2019). Preanalytical aspects on short- and long-term storage of serum and plasma. *Diagnosis (Berl)*, *6*(1), 51-56. https://doi.org/10.1515/dx-2018-0037

Guo, H., Weng, W., Zhang, S., Rinderknecht, H., Braun, B., Breinbauer, R., Gupta, P., Kumar, A., Ehnert, S., Histing, T., Nussler, A. K., & Aspera-Werz, R. H. (2022). Maqui Berry and Ginseng Extracts Reduce Cigarette Smoke-Induced Cell Injury in a 3D Bone Co-Culture Model. *Antioxidants (Basel)*, *11*(12). https://doi.org/10.3390/antiox11122460

Hadjidakis, D. J., & Androulakis, II. (2006). Bone remodeling. *Ann N Y Acad Sci*, *1092*, 385-396. https://doi.org/10.1196/annals.1365.035

Hannemann, J., Laing, A., Middleton, B., Schwedhelm, E., Marx, N., Federici, M., Kastner, M., Skene, D. J., & Boger, R. (2024). Effect of oral melatonin treatment on insulin resistance and diurnal blood pressure variability in night shift workers. A double-blind, randomized, placebo-controlled study. *Pharmacol Res*, *199*, 107011. https://doi.org/10.1016/j.phrs.2023.107011

Harada, S., & Rodan, G. A. (2003). Control of osteoblast function and regulation of bone mass. *Nature*, *423*(6937), 349-355. https://doi.org/10.1038/nature01660

Hardin, P. E., Hall, J. C., & Rosbash, M. (1990). Feedback of the Drosophila period gene product on circadian cycling of its messenger RNA levels. *Nature*, *343*(6258), 536-540. https://doi.org/10.1038/343536a0

Hastings, M. H., Maywood, E. S., & Brancaccio, M. (2018). Generation of circadian rhythms in the suprachiasmatic nucleus. *Nat Rev Neurosci*, *19*(8), 453-469. https://doi.org/10.1038/s41583-018-0026-z

Haus, E. L., & Smolensky, M. H. (2013). Shift work and cancer risk: potential mechanistic roles of circadian disruption, light at night, and sleep deprivation. *Sleep Med Rev*, *17*(4), 273-284. https://doi.org/10.1016/j.smrv.2012.08.003

Haussling, V., Aspera-Werz, R. H., Rinderknecht, H., Springer, F., Arnscheidt, C., Menger, M. M., Histing, T., Nussler, A. K., & Ehnert, S. (2021). 3D Environment Is Required In Vitro to Demonstrate Altered Bone Metabolism Characteristic for Type 2 Diabetics. *Int J Mol Sci*, *22*(6). https://doi.org/10.3390/ijms22062925

Haussling, V., Deninger, S., Vidoni, L., Rinderknecht, H., Ruoss, M., Arnscheidt, C., Athanasopulu, K., Kemkemer, R., Nussler, A. K., & Ehnert, S. (2019). Impact of Four Protein Additives in Cryogels on Osteogenic Differentiation of Adipose-Derived Mesenchymal Stem Cells. *Bioengineering (Basel)*, *6*(3). https://doi.org/10.3390/bioengineering6030067

Javeed, N., & Matveyenko, A. V. (2018). Circadian Etiology of Type 2 Diabetes Mellitus. *Physiology (Bethesda)*, *33*(2), 138-150. https://doi.org/10.1152/physiol.00003.2018

Karsenty, G., & Wagner, E. F. (2002). Reaching a genetic and molecular understanding of skeletal development. *Dev Cell*, *2*(4), 389-406. https://doi.org/10.1016/s1534-5807(02)00157-0

Kasukawa, T., Sugimoto, M., Hida, A., Minami, Y., Mori, M., Honma, S., Honma, K., Mishima, K., Soga, T., & Ueda, H. R. (2012). Human blood metabolite

timetable indicates internal body time. *Proc Natl Acad Sci U S A*, *109*(37), 15036-15041. https://doi.org/10.1073/pnas.1207768109

Kawamoto, D., Ando-Suguimoto, E. S., Bueno-Silva, B., DiRienzo, J. M., & Mayer, M. P. (2016). Alteration of Homeostasis in Pre-osteoclasts Induced by Aggregatibacter actinomycetemcomitans CDT. *Front Cell Infect Microbiol*, *6*, 33. https://doi.org/10.3389/fcimb.2016.00033

Khundmiri, S. J., Murray, R. D., & Lederer, E. (2016). PTH and Vitamin D. *Compr Physiol*, *6*(2), 561-601. https://doi.org/10.1002/cphy.c140071

Kiehn, J. T., Tsang, A. H., Heyde, I., Leinweber, B., Kolbe, I., Leliavski, A., & Oster, H. (2017). Circadian Rhythms in Adipose Tissue Physiology. *Compr Physiol*, *7*(2), 383-427. https://doi.org/10.1002/cphy.c160017

Kikyo, N. (2024). Circadian Regulation of Bone Remodeling. *Int J Mol Sci*, *25*(9). https://doi.org/10.3390/ijms25094717

Krebs, H. A. (1950). Chemical composition of blood plasma and serum. *Annu Rev Biochem*, *19*, 409-430. https://doi.org/10.1146/annurev.bi.19.070150.002205

Kular, J., Tickner, J., Chim, S. M., & Xu, J. (2012). An overview of the regulation of bone remodelling at the cellular level. *Clin Biochem*, *45*(12), 863-873. https://doi.org/10.1016/j.clinbiochem.2012.03.021

Kulik-Rechberger, B., & Kozlowska, M. (2024). Osteoprotegerin and receptor activator of the nuclear factor kappa B ligand (RANKL) in healthy pubertal girls - relationships with physical growth and classical bone turnover markers. *J Physiol Pharmacol*, *75*(1). https://doi.org/10.26402/jpp.2024.1.06

Landgraf, D., Koch, C. E., & Oster, H. (2014). Embryonic development of circadian clocks in the mammalian suprachiasmatic nuclei. *Front Neuroanat*, *8*, 143. https://doi.org/10.3389/fnana.2014.00143

Li, H., Hong, S., Qian, J., Zheng, Y., Yang, J., & Yi, Q. (2010). Cross talk between the bone and immune systems: osteoclasts function as antigen-presenting cells and activate CD4+ and CD8+ T cells. *Blood*, *116*(2), 210-217. https://doi.org/10.1182/blood-2009-11-255026

Liang, X., & FitzGerald, G. A. (2017). Timing the Microbes: The Circadian Rhythm of the Gut Microbiome. *J Biol Rhythms*, *32*(6), 505-515. https://doi.org/10.1177/0748730417729066

Liljander, A., Bejon, P., Mwacharo, J., Kai, O., Ogada, E., Peshu, N., Marsh, K., & Farnert, A. (2011). Clearance of asymptomatic P. falciparum Infections Interacts with the number of clones to predict the risk of subsequent malaria in Kenyan children. *PLoS One*, *6*(2), e16940. https://doi.org/10.1371/journal.pone.0016940

Liu, Y., Berendsen, A. D., Jia, S., Lotinun, S., Baron, R., Ferrara, N., & Olsen, B. R. (2012). Intracellular VEGF regulates the balance between osteoblast and adipocyte differentiation. *J Clin Invest*, *122*(9), 3101-3113. https://doi.org/10.1172/JCI61209

Lunde, L. K., Skare, O., Mamen, A., Sirnes, P. A., Aass, H. C. D., Ovstebo, R., Goffeng, E., Matre, D., Nielsen, P., Heglum, H. S. A., Hammer, S. E., & Skogstad, M. (2020). Cardiovascular Health Effects of Shift Work with Long Working Hours and Night Shifts: Study Protocol for a Three-Year

Prospective Follow-Up Study on Industrial Workers. *Int J Environ Res Public Health*, *17*(2). https://doi.org/10.3390/ijerph17020589

Luo, B., Zhou, X., Tang, Q., Yin, Y., Feng, G., Li, S., & Chen, L. (2021). Circadian rhythms affect bone reconstruction by regulating bone energy metabolism. *J Transl Med*, *19*(1), 410. https://doi.org/10.1186/s12967-021-03068-x

Lutter, A. H., Hempel, U., Wolf-Brandstetter, C., Garbe, A. I., Goettsch, C., Hofbauer, L. C., Jessberger, R., & Dieter, P. (2010). A novel resorption assay for osteoclast functionality based on an osteoblast-derived native extracellular matrix. *J Cell Biochem*, *109*(5), 1025-1032. https://doi.org/10.1002/jcb.22485

Malm, L., Tybring, G., Moritz, T., Landin, B., & Galli, J. (2016). Metabolomic Quality Assessment of EDTA Plasma and Serum Samples. *Biopreserv Biobank*, *14*(5), 416-423. https://doi.org/10.1089/bio.2015.0092

Matson, D. R., Denu, R. A., Zasadil, L. M., Burkard, M. E., Weaver, B. A., Flynn, C., & Stukenberg, P. T. (2021). High nuclear TPX2 expression correlates with TP53 mutation and poor clinical behavior in a large breast cancer cohort, but is not an independent predictor of chromosomal instability. *BMC Cancer*, *21*(1), 186. https://doi.org/10.1186/s12885-021-07893-7

McElderry, J. D., Zhao, G., Khmaladze, A., Wilson, C. G., Franceschi, R. T., & Morris, M. D. (2013). Tracking circadian rhythms of bone mineral deposition in murine calvarial organ cultures. *J Bone Miner Res*, *28*(8), 1846-1854. https://doi.org/10.1002/jbmr.1924

McMillian, M. K., Li, L., Parker, J. B., Patel, L., Zhong, Z., Gunnett, J. W., Powers, W. J., & Johnson, M. D. (2002). An improved resazurin-based cytotoxicity assay for hepatic cells. *Cell Biol Toxicol*, *18*(3), 157-173. https://doi.org/10.1023/a:1015559603643

Minkin, C. (1982). Bone acid phosphatase: tartrate-resistant acid phosphatase as a marker of osteoclast function. *Calcif Tissue Int*, *34*(3), 285-290. https://doi.org/10.1007/BF02411252

Montali, M., Barachini, S., Panvini, F. M., Carnicelli, V., Fulceri, F., Petrini, I., & Pacini, S. (2016). Growth Factor Content in Human Sera Affects the Isolation of Mesangiogenic Progenitor Cells (MPCs) from Human Bone Marrow. *Front Cell Dev Biol*, *4*, 114. https://doi.org/10.3389/fcell.2016.00114

Murck, H., & Steiger, A. (1998). Mg2+ reduces ACTH secretion and enhances spindle power without changing delta power during sleep in men -- possible therapeutic implications. *Psychopharmacology (Berl)*, *137*(3), 247-252. https://doi.org/10.1007/s002130050617

Nakagawa, M., Bando, Y., Nagao, T., Morimoto, M., Takai, C., Ohnishi, T., Honda, J., Moriya, T., Izumi, K., Takahashi, M., Sasa, M., & Tangoku, A. (2011). Expression of p53, Ki-67, E-cadherin, N-cadherin and TOP2A in triple-negative breast cancer. *Anticancer Res*, *31*(6), 2389-2393. https://www.ncbi.nlm.nih.gov/pubmed/21737670

Neves, A. R., Albuquerque, T., Quintela, T., & Costa, D. (2022). Circadian rhythm and disease: Relationship, new insights, and future perspectives. *J Cell Physiol*, *237*(8), 3239-3256. https://doi.org/10.1002/jcp.30815

Niehoff, J., Matzkies, M., Nguemo, F., Hescheler, J., & Reppel, M. (2021). The influence of melatonin on the heart rhythm - An in vitro simulation with

murine embryonic stem cell derived cardiomyocytes. *Biomed Pharmacother*, *136*, 111245. https://doi.org/10.1016/j.biopha.2021.111245

Ono, T., & Nakashima, T. (2018). Recent advances in osteoclast biology. *Histochem Cell Biol*, *149*(4), 325-341. https://doi.org/10.1007/s00418-018-1636-2

Pan, A., Schernhammer, E. S., Sun, Q., & Hu, F. B. (2011). Rotating night shift work and risk of type 2 diabetes: two prospective cohort studies in women. *PLoS Med*, *8*(12), e1001141. https://doi.org/10.1371/journal.pmed.1001141

Patke, A., Young, M. W., & Axelrod, S. (2020). Molecular mechanisms and physiological importance of circadian rhythms. *Nat Rev Mol Cell Biol*, *21*(2), 67-84. https://doi.org/10.1038/s41580-019-0179-2

Ponzetti, M., & Rucci, N. (2021). Osteoblast Differentiation and Signaling: Established Concepts and Emerging Topics. *Int J Mol Sci*, *22*(13). https://doi.org/10.3390/ijms22136651

Qin, Y., Chen, Z. H., Wu, J. J., Zhang, Z. Y., Yuan, Z. D., Guo, D. Y., Chen, M. N., Li, X., & Yuan, F. L. (2023). Circadian clock genes as promising therapeutic targets for bone loss. *Biomed Pharmacother*, *157*, 114019. https://doi.org/10.1016/j.biopha.2022.114019

Rahman, S. A., Wright, K. P., Jr., Lockley, S. W., Czeisler, C. A., & Gronfier, C. (2019). Characterizing the temporal Dynamics of Melatonin and Cortisol Changes in Response to Nocturnal Light Exposure. *Sci Rep*, *9*(1), 19720. https://doi.org/10.1038/s41598-019-54806-7

Reinke, H., & Asher, G. (2016). Circadian Clock Control of Liver Metabolic Functions. *Gastroenterology*, *150*(3), 574-580. https://doi.org/10.1053/j.gastro.2015.11.043

Rico-Llanos, G. A., Becerra, J., & Visser, R. (2017). Insulin-like growth factor-1 (IGF-1) enhances the osteogenic activity of bone morphogenetic protein-6 (BMP-6) in vitro and in vivo, and together have a stronger osteogenic effect than when IGF-1 is combined with BMP-2. *J Biomed Mater Res A*, *105*(7), 1867-1875. https://doi.org/10.1002/jbm.a.36051

Rodriguez-Ezpeleta, N., Teijeiro, S., Forget, L., Burger, G., & Lang, B. F. (2009). Construction of cDNA libraries: focus on protists and fungi. *Methods Mol Biol*, *533*, 33-47. https://doi.org/10.1007/978-1-60327-136-3_3

Rosenwasser, A. M., & Turek, F. W. (2015). Neurobiology of Circadian Rhythm Regulation. *Sleep Med Clin*, *10*(4), 403-412. https://doi.org/10.1016/j.jsmc.2015.08.003

Ruoss, M., Rebholz, S., Weimer, M., Grom-Baumgarten, C., Athanasopulu, K., Kemkemer, R., Kass, H., Ehnert, S., & Nussler, A. K. (2020). Development of Scaffolds with Adjusted Stiffness for Mimicking Disease-Related Alterations of Liver Rigidity. *J Funct Biomater*, *11*(1). https://doi.org/10.3390/jfb11010017

Sahin, S., Isik Gonul, I., Cakir, A., Seckin, S., & Uluoglu, O. (2016). Clinicopathological Significance of the Proliferation Markers Ki67, RacGAP1, and Topoisomerase 2 Alpha in Breast Cancer. *Int J Surg Pathol*, *24*(7), 607-613. https://doi.org/10.1177/1066896916653211

Schilperoort, M., Bravenboer, N., Lim, J., Mletzko, K., Busse, B., van Ruijven, L., Kroon, J., Rensen, P. C. N., Kooijman, S., & Winter, E. M. (2020). Circadian disruption by shifting the light-dark cycle negatively affects bone health in mice. *FASEB J*, *34*(1), 1052-1064. https://doi.org/10.1096/fj.201901929R

Sharma, A., Laurenti, M. C., Dalla Man, C., Varghese, R. T., Cobelli, C., Rizza, R. A., Matveyenko, A., & Vella, A. (2017). Glucose metabolism during rotational shift-work in healthcare workers. *Diabetologia*, *60*(8), 1483-1490. https://doi.org/10.1007/s00125-017-4317-0

Siddiqui, J. A., & Partridge, N. C. (2016). Physiological Bone Remodeling: Systemic Regulation and Growth Factor Involvement. *Physiology (Bethesda)*, *31*(3), 233-245. https://doi.org/10.1152/physiol.00061.2014

Skehan, P., Storeng, R., Scudiero, D., Monks, A., McMahon, J., Vistica, D., Warren, J. T., Bokesch, H., Kenney, S., & Boyd, M. R. (1990). New colorimetric cytotoxicity assay for anticancer-drug screening. *J Natl Cancer Inst*, *82*(13), 1107-1112. https://doi.org/10.1093/jnci/82.13.1107

Staub, J. F., Tracqui, P., Brezillon, P., Milhaud, G., & Perault-Staub, A. M. (1988). Calcium metabolism in the rat: a temporal self-organized model. *Am J Physiol*, *254*(1 Pt 2), R134-149. https://doi.org/10.1152/ajpregu.1988.254.1.R134

Swanson, C., Shea, S. A., Wolfe, P., Markwardt, S., Cain, S. W., Munch, M., Czeisler, C. A., Orwoll, E. S., & Buxton, O. M. (2017). 24-hour profile of serum sclerostin and its association with bone biomarkers in men. *Osteoporos Int*, *28*(11), 3205-3213. https://doi.org/10.1007/s00198-017-4162-5

Swanson, C. M., Kohrt, W. M., Buxton, O. M., Everson, C. A., Wright, K. P., Jr., Orwoll, E. S., & Shea, S. A. (2018). The importance of the circadian system & sleep for bone health. *Metabolism*, *84*, 28-43. https://doi.org/10.1016/j.metabol.2017.12.002

Swanson, C. M., Shea, S. A., Wolfe, P., Cain, S. W., Munch, M., Vujovic, N., Czeisler, C. A., Buxton, O. M., & Orwoll, E. S. (2017). Bone Turnover Markers After Sleep Restriction and Circadian Disruption: A Mechanism for Sleep-Related Bone Loss in Humans. *J Clin Endocrinol Metab*, *102*(10), 3722-3730. https://doi.org/10.1210/jc.2017-01147

Tsang, A. H., Barclay, J. L., & Oster, H. (2014). Interactions between endocrine and circadian systems. *J Mol Endocrinol*, *52*(1), R1-16. https://doi.org/10.1530/JME-13-0118

van der Spoel, E., Oei, N., Cachucho, R., Roelfsema, F., Berbee, J. F. P., Blauw, G. J., Pijl, H., Appelman-Dijkstra, N. M., & van Heemst, D. (2019). The 24-hour serum profiles of bone markers in healthy older men and women. *Bone*, *120*, 61-69. https://doi.org/10.1016/j.bone.2018.10.002

Veis, D. J., & O'Brien, C. A. (2023). Osteoclasts, Master Sculptors of Bone. *Annu Rev Pathol*, *18*, 257-281. https://doi.org/10.1146/annurev-pathmechdis-031521-040919

Vitaterna, M. H., Shimomura, K., & Jiang, P. (2019). Genetics of Circadian Rhythms. *Neurol Clin*, *37*(3), 487-504. https://doi.org/10.1016/j.ncl.2019.05.002

Weng, W., Haussling, V., Aspera-Werz, R. H., Springer, F., Rinderknecht, H., Braun, B., Kuper, M. A., Nussler, A. K., & Ehnert, S. (2020). Material-Dependent Formation and Degradation of Bone Matrix-Comparison of Two Cryogels. *Bioengineering (Basel)*, *7*(2). https://doi.org/10.3390/bioengineering7020052

Weng, W., Zanetti, F., Bovard, D., Braun, B., Ehnert, S., Uynuk-Ool, T., Histing, T., Hoeng, J., Nussler, A. K., & Aspera-Werz, R. H. (2021). A simple method for decellularizing a cell-derived matrix for bone cell cultivation and differentiation. *J Mater Sci Mater Med*, *32*(9), 124. https://doi.org/10.1007/s10856-021-06601-y

Wildemann, B., Lubberstedt, M., Haas, N. P., Raschke, M., & Schmidmaier, G. (2004). IGF-I and TGF-beta 1 incorporated in a poly(D,L-lactide) implant coating maintain their activity over long-term storage-cell culture studies on primary human osteoblast-like cells. *Biomaterials*, *25*(17), 3639-3644. https://doi.org/10.1016/j.biomaterials.2003.10.058

Wu, M., Chen, G., & Li, Y. P. (2016). TGF-beta and BMP signaling in osteoblast, skeletal development, and bone formation, homeostasis and disease. *Bone Res*, *4*, 16009. https://doi.org/10.1038/boneres.2016.9

Xiao, Y. T., Xiang, L. X., & Shao, J. Z. (2007). Bone morphogenetic protein. *Biochem Biophys Res Commun*, *362*(3), 550-553. https://doi.org/10.1016/j.bbrc.2007.08.045

Xie, F., Wang, J., & Zhang, B. (2023). RefFinder: a web-based tool for comprehensively analyzing and identifying reference genes. *Funct Integr Genomics*, *23*(2), 125. https://doi.org/10.1007/s10142-023-01055-7

Ze, Y., Wu, Y., Tan, Z., Li, R., Li, R., Gao, W., & Zhao, Q. (2025). Signaling pathway mechanisms of circadian clock gene Bmal1 regulating bone and cartilage metabolism: a review. *Bone Res*, *13*(1), 19. https://doi.org/10.1038/s41413-025-00403-6

Zhu, S., Ehnert, S., Rouss, M., Haussling, V., Aspera-Werz, R. H., Chen, T., & Nussler, A. K. (2018). From the Clinical Problem to the Basic Research-Co-Culture Models of Osteoblasts and Osteoclasts. *Int J Mol Sci*, *19*(8). https://doi.org/10.3390/ijms19082284

Zvonic, S., Ptitsyn, A. A., Kilroy, G., Wu, X., Conrad, S. A., Scott, L. K., Guilak, F., Pelled, G., Gazit, D., & Gimble, J. M. (2007). Circadian oscillation of gene expression in murine calvarial bone. *J Bone Miner Res*, *22*(3), 357-365. https://doi.org/10.1359/jbmr.061114

7. Declaration

The study was conducted entirely at the Siegfried Weller Institute (SWI) for Trauma Research, Eberhard-Karls-Universität Tübingen, Tübingen.
Prof. Dr. rer nat. Andreas K. Nüssler, Prof. Dr. sc. hum. Sabrina Ehnert, and I conceived the study. The experimental details were designed by Prof. Dr. sc. hum. Sabrina Ehnert and myself. I performed all the experiments and analyzed the experimental data.

The study was conducted in accordance with the Declaration of Helsinki and approved by the Ethics Committee of the University of Tübingen Number 844/2020B02.

I hereby affirm that, with the exception of the cited references and figures, all figures and results presented in my paper are original works. Furthermore, I confirm that all cited references and figures have been duly cited and that the necessary permissions have been obtained.

I hereby affirm that the title of my paper is "Establishment of an *in vitro* model to analyze the effects of the circadian rhythm on bone metabolism." The work was authored solely by me and has not been submitted for credit in any other degree program. This thesis underwent professional linguistic editing provided by the commercial service (Proof-Reading-Service.com).

Place/date/signature of doctoral candidate

8. Acknowledgements

I would like to thank everyone who helped me with this experiment and writing my thesis.

First and foremost, I would like to thank Prof. Dr. rer. nat. Andreas K. Nüssler and Prof. Dr. sc. hum. Sabrina Ehnert. I am very grateful for their help while I performed my experiments and wrote my thesis at SWI. Prof. Dr. rer. nat. Andreas K. Nüssler provided me with a quiet and stable environment to perform my experiments and to write my thesis.
I am very thankful to Prof. Sabrina Ehnert for her continous support during my thesis, her advice and guidance. Her input allowed my experiments to proceed smoothly. Indeed, I would not have been able to successfully complete my project without her help.

I am very grateful to work with all my colleagues who I met during my work at SWI—Romina, Svetlana, Kevin, Bianca, Majd, Engin, Filiz, Maximilian, Jakob, Oliver, Julian, Melike, Alana, Nicolas, Lea, Olivia, and Jimmy—for their help during the experiments and while writing my thesis. Likewise, I would like to express my sincere gratitude to my Chinese colleagues—Guanqiao Chen, Yuxuan Xin, Pengcheng Zhou, Ruizhuo Zhang, and Sanhuan Yuan—for their help in life and work.

Finally, I would like to thank my family in China—my wife Qihan Zeng, who saved my life, keeps supporting my career and is the most important person for me, and my roommate Kejan—for their care and help, I also want to thank the help from the Xiaohui Hu who is one of my friedns in China, who helped me a lot. Thank you all.